EHBP1 and EHD2 regulate Dll4 caveolin-mediated endocytosis during blood vessel development

Amelia M Webb[1], Caitlin R Francis[1], Jayson M Webb[1], Hayle Kincross[1], Keanna M Lundy[1], Rachael Judson[1], Dawn Westhoff[2], Stryder M Meadows[2], Erich J Kushner[1*]

[1]Department of Biological Sciences, University of Denver, Denver, CO; [2]Cell and Molecular Biology Department, Tulane University, New Orleans, LA

*Author for correspondence: Erich Kushner
University of Denver
Department of Biological Sciences
Denver, CO 80210
Phone: 303-871-4386
Email: Erich.Kushner@du.edu

Figures: 8 main figures, 4 supplemental figures

Tables: 2

Running Title: EHBP1 and EHD2 regulate Dll4 caveolin-mediated endocytosis

Keywords: Delta-like 4 protein, Notch, blood vessel development, Angiogenesis, Zebrafish, endocytosis, trafficking, transendocytosis

ABSTRACT

Despite the centrality of Delta/Notch signaling to activate lateral inhibition and define tip/stalk cell specification during angiogenesis, many mechanisms are still incompletely understood. Here, we report that the proteins Epsin homology domain protein 2 (EHD2) and EHD2 binding partner 1 (EHBP1) are required for proper angiogenic signaling in endothelial cells (ECs). EHBP1 and EHD2 localize to Delta-like ligand 4 (Dll4) and actin at adherens junctions. Importantly, we demonstrate that Dll4 is internalized via caveolin-dependent endocytosis, which is reliant on both EHBP1 and EHD2. In the absence of EHBP1 and EHD2, Dll4 endocytosis is significantly impaired, leading to blood vessel defects both *in vitro* and *in vivo*. We propose a model wherein EHBP1 and EHD2 regulate Dll4 endocytosis by anchoring its caveolar endocytic pit to the actin cytoskeleton. Overall, this provides mechanistic detail of how Dll4 is endocytosed during Notch activation.

INTRODUCTION

Angiogenesis is the process in which a new blood vessel develops from an existing vascular bed. During this process, in response to a chemotactic gradient, a single endothelial cell (EC) in a group must identify itself as a tip cell[1]. This tip cell will then lead the charge up the VEGF ligand gradient, pulling behind it a trail of stalk cells in the growing vascular sprout [2]. Tip and stalk cells each have distinct morphological and functional identities: the tip is defined by its spiny, branching filopodia reaching forward as the tip migrates; the stalk is defined by its smoothened appearance and suppressive stability[3, 4]. For proper angiogenic growth to proceed, the maintenance of tip/stalk cell specification is paramount. Central to tip/stalk cell specification is the Notch signaling pathway. Notch is a transmembrane protein composed of an extracellular domain (NECD) and an intracellular domain (NICD). ECs with high Notch activation will adopt a stalk cell identity, whereas an EC deficient in Notch or Notch signaling will adopt a tip cell identity[5, 6].

Delta like proteins are transmembrane Notch ligands. The NECD of a Notch presenting cell will bind Delta on an adjacent cell. This Delta/Notch binding elicits two consecutive cleavage events. Obscured within two domains (LNR and HD) of Notch is a cleavage site termed S2. When exposed, the S2 cleavage site is cleaved by a disintegrin and metalloprotease (ADAM) complex leaving the NECD attached to Delta[7]. This cleavage event precedes the second cleavage by γ-secretase at the S3 cleavage site to release the NICD. Once freed, the NICD translocates to the nucleus, binding the transcription factor CSL to upregulate downstream genes that promote lateral inhibition[8-10].

One proposed mechanism for this activation of Notch by Delta is the application of a mechanical force generated by Delta/NECD transendocytosis (i.e. endocytosis of both Delta and NECD) to expose the S2 domain. This pulling force has been shown to be on the order of 19 pN per single bond[11] and is necessary to force apart the LNR/HD interaction, thus exposing the S2 site for cleavage and subsequent S3 cleavage. Studies on the mechanical force generated by Delta/Notch to date have only focused on Delta-like ligand 1 (Dll1) in non-endothelial tissue[11-13]. Despite the absolute requirement of Delta-like ligand 4 (Dll4) in angiogenesis, the mechanisms of Dll4 transendocytosis remain unknown.

In mammals, there are 4 Epsin15 homology domain (EHD) proteins that serve as dynamin-related GTPases and ATPases[14]. EHD1-4 are each involved in endocytic processes, although EHD2 stands alone from this group in being the only with a solved crystal structure and the only to interact with caveolae[15]. EHD2 multimerizes through an interaction between the G-domain and the EH domain[15, 16]. The multimerization of EHD2 allows it to form a circular ring around an endocytic vesicle to mediate cleavage[15]. This complex has been shown to localize to Cav1, assisting in caveolin endocytosis through stabilization of the caveolae pit structure formed by hairpin shaped proteins in the membrane[17, 18]. EHD2's binding partner, EHBP1, has been much less well characterized. The NPF motifs of EHBP1

bind the EH domain of EHD2. The CH domain of EHBP1 tethers the EHD2/EHBP1 complex to the cytoskeleton. EHBP1 and EHD2 have been found to regulate the clathrin-mediated endocytosis of Transferrin and Glut4[19, 20]; although, how EHBP1 and EHD2 function in ECs has not been characterized.

In this article, we identify EHD2 and EHBP1 as crucial regulators of Notch activation in ECs through the endocytosis of Dll4. Knockout of EHBP1 and EHD2 in zebrafish produced a significant increase in ectopic sprouts in zebrafish intersomitic vessels (ISVs) during development and a reduction in downstream Notch target Hey2. *In vitro*, EHBP1 and EHD2 localized to plasma membrane-bound Dll4 and actin independently of clathrin. Disruption of caveolin endocytosis resulted in EHBP1 and EHD2 failing to organize around Dll4 as well as loss of Dll4 internalization in ECs. Overall, we demonstrate that EHBP1 and EHD2 regulate Dll4 endocytosis by anchoring caveolar endocytic pits to the actin cytoskeleton.

RESULTS

EHBP1 and EHD2 affect blood vessel development.

To investigate whether EHBP1 and EHD2 play a role in angiogenesis, we first characterized how the loss of EHBP1 or EHD2 affected intersomitic blood vessel (ISV) development in *Danio rerio* (zebrafish). This vessel bed requires tightly regulated tip/stalk cell specification and demonstrates stereotyped morphodynamics, making aberrations in normal blood vessel development relatively obvious[21]. A 4-guide knock out (KO) approach[22] was employed to create F0 KOs in the EHBP1 and EHD2 loci (**Figure 1A**). Due to a multiple gene duplication event in teleosts, EHD2 has two isoforms in zebrafish: EHD2a and EHD2b (**Figure S1A**). Each isoform was targeted individually, as well as in combination and validated for indel formation (**Figure S1B**). Quantification of the proportion of fish with ectopic ISVs in each condition revealed a significant increase in EHBP1 KO fish (18.15%), as well as a significant increase in EHD2a/b knockout fish (21.76%) compared to a scramble control (**Figure 1A,B**) at 48 hours post fertilization (hpf). These results suggest that EHBP1 and EHD2a/b are necessary for normal sprouting behaviors.

Focusing on EHBP1, as this protein is less well characterized, we sought to determine the endogenous expression of EHBP1. Antibodies that detect EHBP1 in zebrafish are not available. To circumvent this, we fused a FLAG epitope to the n-terminal domain of the endogenous EHBP1 locus using CRISPR/Cas9 targeting[23] (**Figure 1C**). Staining for FLAG-EHBP1 endogenous expression revealed that EHBP1 strongly localized to neuronal projections (**Figure 1C**). To determine if EHBP1 was being expressed in ECs we dissociated embryos expressing both FLAG-EHBP1 and a GFP-endothelial reporter at 48hpf and plated individual ECs on a dish. We found there was indeed EHBP1 expression in ECs at this time point (**Figure 1D**). EHD2b was detected using *in situ* hybridization and demonstrated a similar expression pattern to EHBP1 along neuronal projections[24] (**Figure S1A**).

Given the potentially confounding effects of performing a global KO, a floxed EHBP1 transgenic line was also created using CRISPR/cas9-mediated recombination (**Figures 1E, S1C**). In line with our previous observations, endothelial-specific ablation of EHBP1 also resulted in a significant increase in the proportion of fish with ectopic ISVs (**Figure 1E,F**). These results suggest that EHBP1 and EHD2a/b mediate endothelial sprouting behaviors and are required for normal blood vessel development.

EHBP1 and EHD2 modulate Notch signaling in zebrafish

We next tested if vascular abnormalities in EHBP1 and EHD2a/b KO lines were related to Notch activity, as loss of Notch signaling has been previously shown to promote hypersprouting in zebrafish blood vessels[25, 26]. Treatment with the small molecule Notch inhibitor LY-411575 phenocopied the increase in ectopic sprouting observed in EHBP1 and EHD2 KOs (**Figure 2A, B**), suggesting that KO of EHBP1 or EHD2 may be detrimental to Notch

signaling. We also observed an elevated number of filopodial projections characteristic of tip cell identity[3] in the LY-411575 treated fish (**Figure 2A, C**). The 4-guide KO injections for EHBP1 or EHD2a/b were repeated and the number of filopodia per ISV were quantified in a tg(kdrl:LifeAct-eGFP) line as performed above. KO of EHBP1, EHD2a, EHD2b, and EHD2a/b did not result in a significant increase in filopodia compared to a scramble control (**Figure 2D, E**), likely due a less severe Notch deactivation compared with LY-411575. To explore Notch activation, expression of Hey2, a downstream Notch target, was monitored in the absence of EHBP1 and EHD2a/b in reference to a GAPDH control. We observed significantly decreased expression of Hey2 in EHBP1, EHD2b, and EHD2a/b KO lines in comparison with the scramble control (**Figure 2F**), further supporting a Notch loss-of-function phenotype in the absence of EHBP1 and EHD2a/b.

In canonical tip/stalk cells specification, tip cells exhibit elevated Dll4 levels that, in turn, elicit repressive Notch activation in the trailing stalk cells[5, 6, 27-30]. Given that KO of EHBP1 or EHD2a/b promoted a Notch loss-of-function phenotype, we hypothesized that these proteins may influence hierarchical tip/stalk cell positioning. To determine how EHBP1 and EHD2 function during tip/stalk cell specification we developed GFP tagged EHBP1 and EHD2 fusion proteins that were injected into a WT line to produce mosaic ISVs to track individual ECs in the sprout collective (**Figure 2G**). Zebrafish EHBP1 and EHD2a/b protein are approximately 70% identical to the Human ortholog, thus predicted to work similarly (**Figure S2**). We reasoned that if EHBP1 or EHD2 did not affect Notch activation there would be a equal EC contribution in tip or stalk cell positions. Confirming this, we injected a control tg(5xUAS:LifeAct-GFP) construct and observed mosaic integration with an even 50/50 distribution between tip and stalk ECs in growing ISVs at 24hpf (**Figure 2G**). However, ECs expressing GFP-EHD2 (tg(5xUAS:GFP-EHD2)) demonstrated a significant bias toward the tip cell position with 76.9% of ISVs exhibiting EHD2-overexpressing ECs in the tip position (**Figure 2G**). Similarly, GFP-EHBP1-expressing ECs showed a 61.5% bias to the tip cell position in ISVs at 24hpf (**Figure 2G**). These results support the role of EHBP1 and EHD2 in Notch activation, suggesting that EHBP1 and EHD2 may play a role in tip cell-related signaling.

EHBP1, EHD2, and actin surround Dll4 at adherens junctions independent of clathrin

EHBP1 and EHD2 have been shown to be involved in endocytic trafficking pathways, both clathrin-dependent and independent[15, 16, 19, 20]. Also, given the effect of EHBP1 and EHD2 on Notch activation and tip cell preference *in vivo*, we hypothesized that EHBP1 and EHD2 were involved in Dll4 endocytosis. To address this, we first focused only on the extracellular pool of Dll4 inserted into the membrane that would be available for Notch binding. To specifically label this bioactive Dll4 pool we constructed a pHluorin tagged Dll4 adenoviral vector. PHluorin is a GFP variant that fluoresces at neutral pH and is quenched when internalized into low pH acidic vesicles allowing for visualization of the extracellular, membrane bound Dll4 population[31] (**Figure 3A**). Co-expression of pHluorin-Dll4 and tagRFP-EHBP1 in ECs showed that EHBP1 clustered around sites of membranous Dll4 (**Figure 3B**). A similar pattern was observed for EHD2, where EHD2 clustered around Dll4 puncta (**Figure 3C**). These results support the potential role of EHBP1 in Dll4 endocytosis. However, staining for endogenous clathrin revealed that clathrin was largely divorced from Dll4 sites as well as EHBP1 and EHD2 (**Figure 3B,C**), suggesting that Dll4 endocytosis employed a clathrin-independent pathway. Both EHBP1 and EHD2 demonstrated a strong association with F-actin bundles around membranous Dll4 as previously reported[19], but clathrin was largely absent in these areas (**Figure 3D-G**). This localization was ablated in ECs treated with actin inhibitors chytochalasin B (**Figure 3H**) or latrunculin A (**Figure 3I**). In ECs with either inhibitor, localization of EHBP1 and EHD2 became diffuse and non-specific (**Figure 3H, I**). At select sites where actin junctions remained, there was a slight localization of EHBP1 and EHD2. In aggregate, these

data suggest that both EHBP1 and EHD2 are associated with membranous Dll4 and actin filaments independent of clathrin, suggesting a clathrin-independent means of endocytosis.

We next explored the notion that EHBP1 and EHD2 are coordinating Dll4 endocytosis through caveolin endocytosis. EHD2 has previously been shown to act as a dynamin-like ATPase driving the scission of caveolar endocytic pits from the membrane, although this role has not been linked to Dll4, EHBP1, or actin-tethering. TagRFP-EHBP1 and caveolin1 both formed around clusters of pHluorin-Dll4 on the membrane (**Figure 4A**). Equally, tagRFP-EHD2 and caveolin 1 also formed around pHluorin-Dll4 on the membrane (**Figure 4B**). TagRFP-EHD2 and caveolin1 both formed clusters of rosettes around the Dll4 on the membrane (**Figure 4B**). To determine if this colocalization was indicative of caveolar endocytosis, we used the cholesterol inhibitor methyl-β-cyclodextrin (MβCD) to inhibit caveolar assembly. Caveolin-1 in ECs treated with MβCD failed to form canonical rosettes and instead was structurally indistinct throughout the cell (**Figure 4C, D**). EHBP1 and EHD2 also lost much of the structural definition and failed to organize around Dll4 (**Figure 4C, D**). These results suggest that EHBP1 and EHD2 mediate Dll4 internalization through caveolin-mediated endocytosis.

To validate the coordination of actin, EHBP1, EHD2, and caveolin-1 to regulate Dll4 endocytosis in an angiogenic sprout, we employed a 3D sprouting assay[32] (**Figure 5A**). EHBP1 colocalized strongly with actin in 3D sprouts consistent with reports that EHBP1 tethers actin through its CH domain (**Figure 5B**). This localization was disrupted in sprouts treated with EHD2 siRNA (si) suggesting that EHD2 plays a role in either recruiting EHBP1 to actin or in stabilizing the bond (**Figure 5C)**. EHBP1 displayed a strong affinity to the adherens junction in the 3D sprout, which was severely disrupted in EHD2si treated ECs (**Figure 5D, E**). Equally, EHD2 strongly localized to adherens junctions which were disrupted in EHBP1si treated cells (**Figure 5F, G**). This localization supports the notion that EHBP1 and EHD2 are present at junctional sites of Dll4/Notch1 binding and therefore likely involved in Dll4/Notch1 transendocytosis. In P6 mouse retinal blood vessels, caveolin strongly colocalized with Dll4 at adherens junctions (**Figure 5H**). Taken together, these results support the cooperative role of EHBP1 and EHD2 acting with caveolin to tether Dll4 endocytic pits to the actin cytoskeleton at the junction between tip and stalk cells.

EHBP1 and EHD2 are required for Dll4/Notch transendocytosis

With evidence of EHBP1 and EHD2 working together to anchor Dll4-containing caveolar pits to the cytoskeleton, we next sought to characterize Dll4 endocytic defects resulting from loss of EHBP1 or EHD2. To do so, a Dll4 antibody was linked to pHrodo, a pH sensitive dye that increases fluorescent intensity with increasing endosomal pH[33]to label extracellular Dll4, and then monitor live Dll4 endocytosis (**Figure 6A, Figure S4**). Pulse-chased with the pHrodo-Dll4 in control ECs, there was a sharp peak in fluorescent intensity at the 10-minute time point (**Figure 6B**). This internalization event was significantly reduced in EHBP1si, EHD2si, and combination EHBP1/EHD2si treated groups (**Figure 6B**). Equally, internalization of pHrodo-Dll4 in ECs treated with the pan-endocytosis inhibitor Dynasore or cholesterol inhibitor MβCD was also significantly reduced (**Figure 6C**). These results suggest that internalization of Dll4 requires EHBP1 and EHD2 and is caveolin dependent.

To more specifically test the Notch/Dll4 binding interaction, we next pHrodo-labelled a recombinant NECD protein. During physiological Dll4/Notch1 binding, the NECD would be attached to the adjacent Dll4-presenting cell prior to S2 cleavage. To reproduce this, we functionalized the pHrodo-labeled NECD to a microbead as previously reported[12] (**Figure 6D**). The kinetics of internalization were slightly delayed in scramble-treated ECs compared to the Dll4-antibody internalization likely due to the presence of a bead tether (**Figure 6E**); however, baseline internalization was significantly impaired by treatment in EHBP1si, EHD2si, or EHBP1/EHD2si combination groups (**Figure 6E**). The same internalization defect was also observed in Dll4si, Jag1si, and dual Dll4 and Jag1si treated ECs, suggesting NECD binding was

specific to these Notch ligands (**Figure 6F**). Overall these data indicate that EHBP1 and EHD2 are required for Dll4 endocytosis.

We considered that the disruptions in Dll4 endocytosis may be due to reduced Dll4 bioavailability. However, we observed that EHBP1si, EHD2si, DAPT, or Dynasore treatment did not affect Dll4 levels (**Figure 6G, H**). Therefore, the reduced internalization of Dll4 is a direct result of loss of EHBP1 and EHD2, supporting their role as endocytic mediators of Dll4/Notch1 transendocytosis. In order to visualize this endocytic impairment in the absence of EHBP1 and EHD2 we employed TEM imaging. Both EHBP1 and EHD2 knockdown greatly increased the number of small endocytic vacuoles near the plasma membrane (**Figure 6I**), an observation consistent with previous reports[15, 34] in which caveolae are unable to be stabilized through actin anchoring and accumulate near the plasma membrane.

RNA-seq analysis of EHBP1 deficient cells

EHD2 has been previously characterized in other cell types[15, 16, 19]; however, very little is generally known about EHBP1's function, particularly in endothelial tissues. To gain better insight into EHBP1's role in endothelial signaling we preformed RNA-seq analysis. Confirmation of KD efficiency was validated by western blot (**Figure 7A**). In the EHBP1si treated group, there were only 99 significantly differentially regulated genes compared to the control (**Table S1**). A volcano plot shows the log-fold-change of gene expression between the scramble and EHBP1si treated ECs, with upregulation presented above the line and downregulation presented below the line (**Figure 7B)**. Of these 99 differentially regulated genes, approximately 45% either contained EGF repeats, analogous to Dll4 and Notch, or were indirectly related to EGF- containing proteins signaling processes (**Figure 7B, C; Table S2**). Further analysis revealed that 8 of the 99 genes were directly related to caveolin endocytosis (**Figure 7B, D**) and 4 of the 99 genes were actin remodeling genes (**Figure7B, E**). This suggests that EHBP1's role in regulating caveolar endocytosis may not be specific to Dll4 but can accommodate a variety of cargo. To determine if this trend translated to an increased consequence to angiogenic signaling, we grouped the differentially regulated genes by gene ontology. 8 genes were directly attributed to either angiogenesis, blood vessel development, or response to hypoxia (**Figure 7F**). Another 11 genes were more broadly attributed to the trafficking ontologies SNARE binding, G protein-coupled receptor binding, exocyst, and MAPK cascade (**Figure 7G**). Beyond these, all differentially regulated gene ontologies are represented in the bar plot and show a dramatic impact on cellular processes as a whole (**Figure 7H**). Overall, EHBP1 shows an affinity for endocytic processes related to EGF-repeat containing proteins, such as Dll4.

DISCUSSION

Although Notch signaling is critical for blood vessel development, endocytic mechanisms that regulate both Dll4 cell surface expression and Notch receptor activation remain elusive. We report that EHBP1 and EHD2 work in concert to regulate Notch signaling through the transendocytosis of the Dll4/Notch1 complex by caveolar endocytosis. Importantly, this is the first characterization of Dll4 as being internalized by caveolin-mediated endocytosis. We also demonstrate that EHBP1 and EHD2 work cooperatively to regulate clathrin-independent endocytosis through tethering to the actin cytoskeleton. In a broader context, our results demonstrate an organotypic trafficking signature that constitutes a novel level of signaling regulation critical to blood vessel formation.

We propose a model wherein EHD2 oligomerizes around the neck of an endocytic vesicle internalizing Dll4 (**Figure 8**). The EH domain of EHD2 also binds to the NPF motifs of EHBP1; EHBP1 is tethered to the actin cytoskeleton, generating the anchoring force necessary to expose the S2 cleavage site of NECD (**Figure 8**). In the absence of EHBP1, the caveolar pit will be incapable to tether to the actin cytoskeleton and the caveolar pit will lose structure provided by the actin support and be unable to generate the force necessary for Dll4/NECD

transendocytosis. In the absence of EHD2, the caveolar pit will lose the ability to perform scission from the membrane in addition to losing the bridge to the actin cytoskeleton through EHBP1. Overall, both EHBP1 and EHD2 provide a key function in immobilizing Dll4-containing endocytic pits during Notch binding interactions.

Dll4 is unquestionably vital for Notch signaling and blood vessel morphogenesis. In a model for Notch activation in other cell types, a mechanical pulling force on the NECD to expose the S2 domain for cleavage is generated by Dll1 endocytosis. After S2 cleavage, the Dll1/NECD complex is internalized and, presumably, targeted for lysosomal degradation. In the adjacent Notch presenting cell, once the S2 is cleaved and the NECD is released, the S3 cleavage by γ-secretase and NICD release can proceed[7]. Others have reported that the Dll1 pulling force is derived from clathrin-dependent endocytosis; however, our results suggest a different pathway. In our investigation, we equally explored the idea that EHBP1 and EHD2 were using clathrin-dependent or independent programs to aid in Dll4 internalization. To our surprise, we did not observe any significant Dll4, EHPB1 or EHD2 colocalization with clathrin in ECs, indicating this was not the operative pathway for Dll4 endocytosis. However, we determined that Dll4 strongly relied on caveolar endocytosis for NECD transendocytosis and subsequent Notch activation. Dll4 being associated with caveolin-mediated endocytosis has not been previously reported and is in contrast from reports investigating Dll1[11, 12, 35, 36]. The reasons for this disparity could be due to both receptor-type and/or tissue source differences.

We used RNA seq analysis to determine how the transcriptional landscape is modified in the absence of EHBP1. Given EHBP1 and EHD2 demonstrate functional dependency (Guillherme et al. 2003), these findings would be predicted to be similar for an EHD2 loss of function analysis. Among the fascinating findings, there was differential expression of gene transcripts related to proteins that contained EGF repeats, such as Notch and Dll4. In one view this is not surprising, given proteins that contain EGF repeats are typically plasma membrane bound receptors or ligands that require endocytosis for general function, such as removal from the plasma membrane, recycling, etc. However, we were surprised at how small and narrow the list of differentially regulated genes were, with approximately 45% of hits relating to EGF repeat-containing proteins. We interpret this data as evidence that EHBP1 may play a very selective role in endocyctosis, assisting internalization of proteins that require a robust pulling force by anchoring endocytic pits to the actin cytoskeleton.

In aggregate, our results characterize EHBP1 and EHD2's role in Dll4 caveolin-mediated endocytosis. Our analysis uncovered two major findings: 1) Dll4 uses a non-clathrin-mediated endocytic program; and 2) EHBP1 and EHD2 are required for Dll4 internalization during Notch receptor engagement. These results raise questions pertaining to the role of other endocytic proteins in the basal- and/or bound-state of Dll4. Additionally, with regard to EHBP1 and EHD2, what is the precise pulling force contribution is required for Dll4 endocytosis and how much is controlled by anchoring to the cytoskeleton is not known. It is also interesting to speculate how the caveolar machinery may interface with modifiers of Dll4, such as fringe proteins known to glycosylate Dll4's extracellular domain. Overall, we believe that in addition to transcriptional regulation of Dll4/Notch proteins, the endocytic machinery involved in their signaling may add yet another level of regulation important for blood vessel development.

ACKNOWLEDGEMENTS
Work was supported by funding from the National Heart Lung Blood Institute (Grant 1R56HL148450-01, R00HL124311) (A.M.W, C.R.F, and E.J.K). We also thank Jennifer Bourne and the Electron Microscopy Center at the University of Colorado Anschutz Medical Campus for assistance with transmission electron micrograph collection.

CONTRIBUTIONS
A.M.W, H.K, K.M.L and E.J.K created zebrafish and cell line constructs. A.M.W and E.J.K conceived experiments. R.J. performed mouse retinal experiments. A.M.W and C.R.F performed fibrin bead experiments. J.M.W and A.M.W performed RNA-seq analysis. S.M.M performed EHD2 TEM analysis. A.M.W. and E.J.K wrote the manuscript.

MATERIALS AND METHODS

Zebrafish Handling

All zebrafish used in this study were AB strain. Zebrafish housing and protocols were all approved by the Institutional Animal Care and Use Committee (IACUC, number 946125-1).

Microinjection

Tol2 transposase RNA was synthesized from pT3TS-Tol2 (Addgene, #31831) using the MEGAscript™ T3 Transcription Kit (Thermo Fisher Scientific, AM1338) and stored at -80℃ at a dilution of 100 ng/µl. Injection mixture was prepared on ice containing 300 ng Tol2 transposase RNA and 500 ng recombinant plasmid was brought to 10 µl total volume with 0.1% phenol-red (VWR, 470301-974) in water. 1-4 cell embryos were injected directly into cell with 2 pL injection mixture.

4-guide CRISPR/Cas9 targeted gene KO was performed as outlined by Wu et al 2018. In brief, 4 single guide RNA templates were synthesized for each target gene using HiScribe™ SP6 RNA Synthesis Kit (New England BioLabs, E2070S). Injection mixture was prepared on ice containing 5 µM Cas9 (PNA Bio, CP02), 1 µg/µL sgRNA, and brought to 6 µL with 0.1% phenol-red in water. Cas9 and sgRNA guides were pre-complexed at 37℃ for 5 mins. 1-4 cell embryos were injected directly into yolk with 2 pL injection mixture.

In Situ Hybridization

In situ hybridization performed as outlined by Thisse and Thisse 2007.

Cell Culture

Glass-bottomed imaging dishes were exposed to UV light for 6 minutes and coated with Poly-D-Lysine (Thermo Fisher Scientific, A3890401) for a minimum of 20 minutes. Dishes were then coated with 15 µg/mL laminin mouse protein (Thermo Fisher Scientific, 23017015) overnight at 37℃. Cells were plated onto laminin coated dishes for 4-6 hours prior to imaging or fixation. 0.9 µM siRNA (Thermo Fisher Scientific, s225944, s26959, am4611) was introduced to primary HUVEC using the Neon® transfection system (Thermo Fisher Scientific).

Adenovirus constructs (tagRFP-EHD2, tagRFP-EHBP1, Emerald-Clathrin) created as previously described (He et al. 1998). In brief, constructs were introduced via Gibson Assembly® (New England BioLabs, E2611) into pShuttle-CMV (Addgene, #16403). PShuttle-CMV plasmids were then digested overnight with MssI (Thermo Fisher Scientific, IVGN0244) and purified using E.N.Z.A.® Gel Extraction Kit (Omega Bio-Tek, D2500-01). Linearized pShuttle-CMV plasmids were transformed into the final viral backbone using electrocompetent AdEasier-1 cells (Addgene, #16399). Successful incorporation of pShuttle-CMV construct into AdEasier-1 cells confirmed via digestion with PacI (Thermo Fisher Scientific, IVGN0184). 5000 ng plasmid was then digested at 37℃ overnight, then 85℃ for 10 minutes and transfected in a 3:1 polyethylenimine (PEI, Sigma Aldrich, 408747):DNA ratio into 70% confluent HEK 293A cells (Thermo Fisher Scientific, R70507) in a T-25 flask (Genesee Scientific, 25-207).

Over the course of approximately 2-4 weeks, fluorescent cells became swollen and burst or budded off of the plate. Once approximately 50% of the cells had lifted off of the plate, cells were scraped off and spun down at 2000 rpm for 5 minutes in a 15 mL conical tube. The supernatant was aspirated, and cells were resuspended in 1 mL DPBS (Genesee Scientific, 25-508B). Cells were then lysed by 3 consecutive quick freeze-thaw cycles in liquid nitrogen, spun down for 5 minutes at 2000 rpm, and supernatant was added to 2 70% confluent T-75 flasks (Genesee Scientific, 25-209). Propagation continued and collection repeated for infection of 10 15 cm dishes. After collection and 4 freeze thaw cycles of virus collected from 10 15 cm dishes, 8 mL viral supernatant was collected and combined with 4.4 g CsCl (Sigma Aldrich, 289329) in 10 mL DPBS. Solution was overlaid with mineral oil and spun at 32,000 rpm at 10℃ for 18 hours. Viral fraction was collected with a syringe and stored in a 1:1 ratio with a storage buffer

containing 10 mM Tris, pH 8.0, 100 mM NaCl, 0.1% BSA, and 50% glycerol. Primary Human Umbilical Vein Endothelial Cells (Promocell, C-12253) were treated with virus for 16 hours at a 1/1000 final dilution in all cell culture experiments.

Fibrin Bead Assay performed according to protocol as outlined by Nakatsu et al. 2007.

pHrodo internalization assay

PHrodo™ iFL Red STP Ester (Thermo Fisher Scientific, P36010) was brought to 10 mM with DMSO. On the day of antibody labeling, pHrodo™ iFL Red STP Ester was diluted to 2 mM in DMSO (VWR Life Science, 97063-136). Antibody was brought up in DPBS (2 mg/mL final concentration for Dll4 polyclonal antibody [Thermo Fisher Scientific, PA5-46974]; 1 mg/mL final concentration for recombinant human Notch-1 Fc Chimera [R&D Systems, P46531]) and added to 1/10 volume 1 M sodium bicarbonate, pH 8.5. 3.3 µL of 2 mM pHrodo™ dye was added to the antibody and allowed to react in the dark for 1 hour with gentle flicking every 15 minutes. While this reaction is occurring, Zeba™ Spin Desalting Column (Thermo Fisher Scientific, 89882) were washed 3 times with 300 µL DPBS at 1500 x g for 1 minute. After 1 hour, the labeled antibody solution was loaded into the desalting column and allowed to absorb. DPBS was overlaid on top of labeled antibody to bring total column load volume to 70 µL and spun at 1500 x g for 2 minutes. Flow-through stored at 4 ℃.

For bead tethered pHrodo, 6 µL of pHrodo-conjugated antibody brought to 200 µL TBST and added to 10 µL of either Dynabeads™ Protein G (Thermo Fisher Scientific, 10004D) or Protein A Agarose Resin (Gold Biotechnology, P-400-5) . Beads and antibody were incubated and rotated at room temperature for 10 minutes. Conjugated beads were washed 3 times with 200 µL TBST then stored in a final volume of 10 µL TBST at 4℃.

3 µL pHrodo labeled antibody and 1 µL Hoechst 33342 trihydrochloride, trihydrate (Thermo Fisher Scientific, H3570) was added to 70-80 percent confluent HUVECs plated on laminin coated dishes in 1 mL media and incubated at 37℃ for 10 minutes. After 10 minutes, the cells were washed 3 times with 1 mL DPBS and then placed in 2 mL media. 10 z-stack images were taken for each condition, this marks time point 0 minutes. After images were taken of each group, cells were returned to 37℃ for 10 minutes and imaged again.

Microscopy

Images were taken on a Nikon Eclipse Ti inverted microscope equipped with a CSU-X1 Yokogawa spinning disk field scanning confocal system and a Hamamatusu EM-CCD digital camera. Cell culture images were captured using a Nikon Plan Apo 60x NA 1.40 oil objective using Olympus type F immersion oil NA 1.518 (ThorLabs, MOIL-30). Fish images were taken using either Nikon Apo LWD 20x NA 0.95 or Nikon Apo LWD 40x NA 1.15 water objectives. For transmission electron microscopy images, primary HUVEC of specified treatment were fixed in 2% glutaraldehyde, 2% PFA, 0.2 M Cacodylate buffer and sent to Jennifer Bourne at the University of Colorado Anschutz Medical Campus.

Immunohistochemistry

2D cell culture was fixed in 4% paraformaldehyde in DPBS for 10 minutes. Cells were then washed 3 times for 5 minutes in TBST and permeabilized in 0.1% Triton-X 100 for 10 minutes. Cells were then washed 3 times for 5 minutes and blocked for 1 hour in 2% bovine serum albumin (BSA). Primary antibodies were applied at specified dilutions in Key Resources Table (Appendix A) overnight. Cells were washed 3 times for 10 minutes in TBST and then moved to secondary for 2 hours at specified dilutions in Key Resources Table. Cells were washed again 3 times for 15 minutes in TBST before imaging.

Western Blot
Primary HUVEC culture was trypsinized and lysed using Ripa buffer (20 mM Tris-HCl [pH 7.5], 150 mM NaCl, 1 mM Na_2EDTA, 1 mM EGTA, 1% NP-40, 1% sodium deoxycholate, 2.5 mM sodium pyrophosphate, 1 mM β-glycerophosphate, 1 mM Na_3VO_4, 1 µg/mL leupeptin) containing 1x ProBlock™ Protease Inhibitor Cocktail -50, Plus EDTA (GoldBio, GB-334-20). Total concentration of protein in lysate was quantified using the Pierce™ BCA Protein Assay Kit (Thermo Fisher Scientific, 23225) measured at 562 nm and compared to a standard curve. 20-50 µg protein was prepared in 0.52 M SDS, 1.2 mM bromothymol blue, 58.6% glycerol, 75 mM Tris pH 6.8, and 0.17 M DTT. Samples were boiled for 10 minutes, then 35 µL was loaded in a 7-12% SDS gel and run at 170 V. Protein was then transferred to Immun-Blot PVDF Membrane (BioRad, 1620177) at 4℃, 100 V for 1 hour 10 minutes. Blots were blocked in 2% milk for 1 hour, then put in primary antibody at specified concentrations overnight. After 3 10-minute washes with TBST, secondary antibodies at specified concentrations were applied for 4 hours. After 3 additional TBST washes, blots were developed with ProSignal® Pico ECL Spray (Genesee Scientific, 20-300S).

Pharmacological Treatment
DAPT (Sigma Aldrich, D5942) was applied to cells for 3 days at a final concentration of 5 µM. Dynasore hydrate (Sigma Aldrich, D7693) was applied to cells for 30 minutes at a final concentration of 100 µM. LY-411575 (Sigma Aldrich, SML0506) was diluted in egg water to a final dilution of 2 µM from 30-48 hpf. Latrunculin A (Sigma Aldrich, 428021-100UG) was applied to cells for 1 hour at a final concentration of . Cytochalasin B (Sigma Aldrich, C6762-5MG) was applied to cells for 1 hour at a final concentration of 10 µM. Methyl-β-Cyclodextrin (Sigma Aldrich, M7439-1G) was applied to cell for 10 minutes at a final concentration of 10 mM.

RNA-Sequencing
RNA collected from siRNA treated HUVEC cells was collected in triplicate and sent to Novogene for RNA-sequencing. Sequence files received from Novogene were processed using the Bioconductor package in R-Studio as described by Love et al. (2015) using Homo Sapiens GRCh38 version 98 as a reference genome.

Quantification and Statistical Analysis
Ectopic vessels were defined by a sprout emerging out of or separate from the defined ISV and quantified in 48 hpf embryos expressing tg(kdrl:GFP). Number of filopodia per ISV was defined by filopodial extensions (observed with zebrafish line tg(fli:LifeAct-GFP)) emerging from a fully formed ISV that has connected with the DLAV. RT-PCR was quantified using the gel analysis function in Fiji image analysis software (Schindelin et al., 2012). In sum, rectangular sections were drawn around individual lanes in gray-scale high-quality gel image using the pathway *Analyze > Gel > Select First Lane*, *Analyze > Gel > Select Next Lane.* After all lanes are selected, the pathway *Analyze > Gel > Plot Lanes*. The peaks of each lane were then segmented using the Straight Line selection tool, and highlighted with the Wand tool. Selection of the area inside the peak generates a Results window with the Area and Percent of each peak. The percent value of each sample was divided by the percent value of the control to obtain a relative density. Relative densities of the gene of interest (e.g. Hes1, Hey1, Hey2) were divided by the relative density of the housekeeping gene (GAPDH) to obtain a final adjusted density value.
Cellular uptake of pHrodo-labeled antibody was also quantified using Fiji image analysis software. Stack files were z-stacked at maximum intensity, and each color channel was adjusted so that the background was zero. Each individual cell was outlined with the Freehand Selections tool. The color channels were then separated and any background fluorescence (488

channel) was subtracted from the pHrodo fluorescent intensity (555 channel) using pathway *Process* > *Image Calculator*. The Integrated Density of pHrodo fluorescent intensity within each cell boundary was then recorded for every cell at each time point. Each experiment was performed in duplicate. All statistical analysis was performed in GraphPad Prism8.

Reagent Type (species) or Resource	Designation	Source or Reference	Identifiers	Additional Information
Antibody	Clathrin Heavy Chain Monoclonal Antibody (Mouse)	Thermo Fisher Scientific	MA1-065	Immunohistochemistry: 1/1000 dilution
Antibody	Caveolin 1 Polyclonal Antibody (Rabbit)	Thermo Fisher Scientific	PA1-064	Immunohistochemistry: 1/2000 dilution
Antibody	Dll4 Polyclonal Antibody (Goat)	Thermo Fisher Scientific	PA5-46974	Immunohistochemistry: 1/1000 dilution
Antibody	Dll4 Polyclonal Antibody (Rabbit)	abcam	ab7280	Immunoblotting: 1/500 dilution
Antibody	Dll4 Polyclonal Antibody (Mouse)	Thermo Fisher Scientific	PA5-46974	
Antibody	EHBP1 Polyclonal Antibody (Rabbit)	Thermo Fisher Scientific	PA5-57282	Immunohistochemistry: 1/500 Dilution
Antibody	EHD2 Polyclonal Antibody (Rabbit)	Thermo Fisher Scientific	PA5-61497	Immunohistochemistry: 1/1000 dilution Immunoblotting: 1/500 dilution
Antibody	Recombinant Anti-alpha Tubulin antibody (Rabbit)	Abcam	ab52866	Immunoblotting: 1/5000 dilution
Antibody	Monoclonal Anti-α-Tubulin antibody (Mouse)	Sigma Aldrich	T9026-.2ML	Immunoblotting: 1/5000 dilution
Antibody	VE-cadherin polyclonal antibody	Enzo Life Sciences	ALX-210-232-C100	Immunostaining: 1/200
Antibody	DYKDDDDK Tag polyclonal antibody	Thermo Fisher Scientific	PA1-984B	Immunostaining: 1/100 dilution
Antibody	Donkey anti-Mouse IgG (H+L) Highly Cross-Absorbed Secondary Antibody, Alexa Fluor 647	Thermo Fisher Scientific	A-31571	Immunostaining: 1/1000 dilution
Antibody	Goat anti-Rabbit IgG (H+L) Highly Cross-Absorbed	Thermo Fisher Scientific	A32733	Immunostaining: 1/1000 dilution

	Secondary Antibody, Alexa Fluor Plus 647			
Antibody	Chicken anti-Rabbit IgG (H+L) Cross-Absorbed Secondary Antibody, Alexa Fluor 647	Thermo Fisher Scientific	A-21443	Immunostaining: 1/1000 dilution
Antibody	Goat anti-Mouse IgG (H+L) Secondary Antibody, HRP	Thermo Fisher Scientific	31430	Immunoblotting: 1/5000 dilution
Antibody	Goat Anti-Rabbit IgG (HL), HRP-Linked Whole Ab	Genesee Scientific	20-303	Immunoblotting: 1/5000
Cellular Dye	Hoechst 33342, trihydrochloride, trihydrate	Thermo Fisher Scientific	H3570	1/1000 dilution cell culture
Cellular Dye	Alexa Fluor™ 647 Phalloidin	Thermo Fisher Scientific	A22287	1/500 dilution cell culture
Recombinant Protein	Recombinant Human Notch-1 Fc Chimera	R&D Systems	P46531	
Chemical compound	Cas9 protein with NLS, high concentration	PNA Bio	CP02	
Chemical compound	Cytochalasin B	Sigma Aldrich	C6762-5MG	
Chemical compound	Dimethyl sulfoxide ≥99.5%, Ultra Pure Grade	VWR Life Science	97063-136	
Chemical compound	LY-411575	Sigma Aldrich	SML0506-5MG	2 μM final concentration
Chemical compound	Latrunculin A	Sigma Aldrich	428021-100UG	5 μM final concentration
Chemical compound	Methyl-β-cyclodextrin	Sigma Aldrich	M7439-1G	10 mM final dilution
Chemical compound	pHrodo™ iFL Red STP Ester (amine-reactive)	Thermo Fisher Scientific	P36010	
Chemical compound	DAPT	Sigma Aldrich	D5942-5MG	5 μM final concentration
Chemical compound	Dynasore hydrate	Sigma Aldrich	D7693-5MG	100 μM final concentration
Chemical compound	Phenol Red	VWR	470301-974	0.1% final dilution in water

Commercial assay or kit	MEGAscript™ T3 Transcription Kit	Thermo Fisher Scientific	AM1338	
Commercial assay or kit	HiScribe™ SP6 RNA Synthesis Kit	New England BioLabs	E2070S	
Commercial assay or kit	High Capacity cDNA Reverse Transcription Kit	Thermo Fisher Scientific	4368814	
Other	Dynabeads™ Protein G for Immunoprecipitation	Thermo Fisher Scientific	10004D	
Other	Protein A Agarose Resin	Gold Biotechnology	P-400-5	
Other	Poly-D-Lysine	Thermo Fisher Scientific	A3890401	
Other	Laminin Mouse Protein, Natural	Thermo Fisher Scientific	23017015	

REFERENCES

1. Chappell, J.C., et al., *Local guidance of emerging vessel sprouts requires soluble Flt-1.* Dev Cell., 2009. **17**(3): p. 377-86. doi: 10.1016/j.devcel.2009.07.011.
2. Chappell, J.C., D.M. Wiley, and V.L. Bautch, *How blood vessel networks are made and measured.* Cells Tissues Organs, 2012. **195**(1-2): p. 94-107.
3. Gerhardt, H., et al., *VEGF guides angiogenic sprouting utilizing endothelial tip cell filopodia.* J Cell Biol., 2003. **161**(6): p. 1163-77. Epub 2003 Jun 16.
4. Ninov, N., M. Borius, and D.Y. Stainier, *Different levels of Notch signaling regulate quiescence, renewal and differentiation in pancreatic endocrine progenitors.* Development, 2012. **139**(9): p. 1557-67.
5. Benedito, R., et al., *The notch ligands Dll4 and Jagged1 have opposing effects on angiogenesis.* Cell, 2009. **137**(6): p. 1124-35.
6. Blanco, R. and H. Gerhardt, *VEGF and Notch in tip and stalk cell selection.* Cold Spring Harb Perspect Med, 2013. **3**(1): p. a006569.
7. Mumm, J.S., et al., *A ligand-induced extracellular cleavage regulates gamma-secretase-like proteolytic activation of Notch1.* Mol Cell, 2000. **5**(2): p. 197-206.
8. Gordon, W.R., K.L. Arnett, and S.C. Blacklow, *The molecular logic of Notch signaling--a structural and biochemical perspective.* J Cell Sci, 2008. **121**(Pt 19): p. 3109-19.
9. Ramasamy, S.K., et al., *Endothelial Notch activity promotes angiogenesis and osteogenesis in bone.* Nature, 2014. **507**(7492): p. 376-380.
10. Pitulescu, M.E., et al., *Dll4 and Notch signalling couples sprouting angiogenesis and artery formation.* Nat Cell Biol, 2017. **19**(8): p. 915-927.
11. Shergill, B., et al., *Optical tweezers studies on Notch: single-molecule interaction strength is independent of ligand endocytosis.* Dev Cell, 2012. **22**(6): p. 1313-20.
12. Meloty-Kapella, L., et al., *Notch ligand endocytosis generates mechanical pulling force dependent on dynamin, epsins, and actin.* Dev Cell, 2012. **22**(6): p. 1299-312.
13. Gessler, M., *Dll1 and Dll4: similar, but not the same.* Blood, 2009. **113**(22): p. 5375-6.
14. Melo, A.A., et al., *Structural insights into the activation mechanism of dynamin-like EHD ATPases.* Proc Natl Acad Sci U S A, 2017. **114**(22): p. 5629-5634.
15. Moren, B., et al., *EHD2 regulates caveolar dynamics via ATP-driven targeting and oligomerization.* Mol Biol Cell, 2012. **23**(7): p. 1316-29.
16. Hoernke, M., et al., *EHD2 restrains dynamics of caveolae by an ATP-dependent, membrane-bound, open conformation.* Proc Natl Acad Sci U S A, 2017. **114**(22): p. E4360-e4369.
17. Torrino, S., et al., *EHD2 is a mechanotransducer connecting caveolae dynamics with gene transcription.* J Cell Biol, 2018. **217**(12): p. 4092-4105.
18. Kovtun, O., et al., *Cavin family proteins and the assembly of caveolae.* J Cell Sci, 2015. **128**(7): p. 1269-78.
19. Guilherme, A., et al., *EHD2 and the novel EH domain binding protein EHBP1 couple endocytosis to the actin cytoskeleton.* J Biol Chem, 2004. **279**(11): p. 10593-605.
20. Guilherme, A., et al., *Role of EHD1 and EHBP1 in perinuclear sorting and insulin-regulated GLUT4 recycling in 3T3-L1 adipocytes.* J Biol Chem, 2004. **279**(38): p. 40062-75.

21. Gore, A.V., et al., *Vascular development in the zebrafish.* Cold Spring Harb Perspect Med, 2012. **2**(5): p. a006684.
22. Wu, R.S., et al., *A Rapid Method for Directed Gene Knockout for Screening in G0 Zebrafish.* Dev Cell, 2018. **46**(1): p. 112-125.e4.
23. Hoshijima, K., M.J. Jurynec, and D.J. Grunwald, *Precise Editing of the Zebrafish Genome Made Simple and Efficient.* Dev Cell, 2016. **36**(6): p. 654-67.
24. Thisse, C. and B. Thisse, *High-resolution in situ hybridization to whole-mount zebrafish embryos.* Nat Protoc, 2008. **3**(1): p. 59-69.
25. Therapontos, C. and N. Vargesson, *Zebrafish notch signalling pathway mutants exhibit trunk vessel patterning anomalies that are secondary to somite misregulation.* Dev Dyn, 2010. **239**(10): p. 2761-8.
26. Siekmann, A.F. and N.D. Lawson, *Notch signalling limits angiogenic cell behaviour in developing zebrafish arteries.* Nature, 2007. **445**(7129): p. 781-4.
27. Ehling, M., et al., *Notch controls retinal blood vessel maturation and quiescence.* Development, 2013. **140**(14): p. 3051-61.
28. Eilken, H.M. and R.H. Adams, *Dynamics of endothelial cell behavior in sprouting angiogenesis.* Curr Opin Cell Biol, 2010. **22**(5): p. 617-25.
29. Gridley, T., *Notch signaling in vascular development and physiology.* Development, 2007. **134**(15): p. 2709-18.
30. Hellstrom, M., et al., *Dll4 signalling through Notch1 regulates formation of tip cells during angiogenesis.* Nature, 2007. **445**(7129): p. 776-80.
31. Sankaranarayanan, S., et al., *The use of pHluorins for optical measurements of presynaptic activity.* Biophys J, 2000. **79**(4): p. 2199-208.
32. Nakatsu, M.N., J. Davis, and C.C. Hughes, *Optimized fibrin gel bead assay for the study of angiogenesis.* J Vis Exp., 2007(3): p. 186. doi: 10.3791/186. Epub 2007 Apr 29.
33. Kamen, L., et al., *A novel method for determining antibody-dependent cellular phagocytosis.* J Immunol Methods, 2019. **468**: p. 55-60.
34. Matthaeus, C., et al., *EHD2-mediated restriction of caveolar dynamics regulates cellular fatty acid uptake.* Proc Natl Acad Sci U S A, 2020. **117**(13): p. 7471-7481.
35. Heuss, S.F., et al., *The intracellular region of Notch ligands Dll1 and Dll3 regulates their trafficking and signaling activity.* Proc Natl Acad Sci U S A, 2008. **105**(32): p. 11212-7.
36. Okano, M., et al., *Mib1 modulates dynamin 2 recruitment via Snx18 to promote Dll1 endocytosis for efficient Notch signaling.* Genes Cells, 2016. **21**(5): p. 425-41.

FIGURES

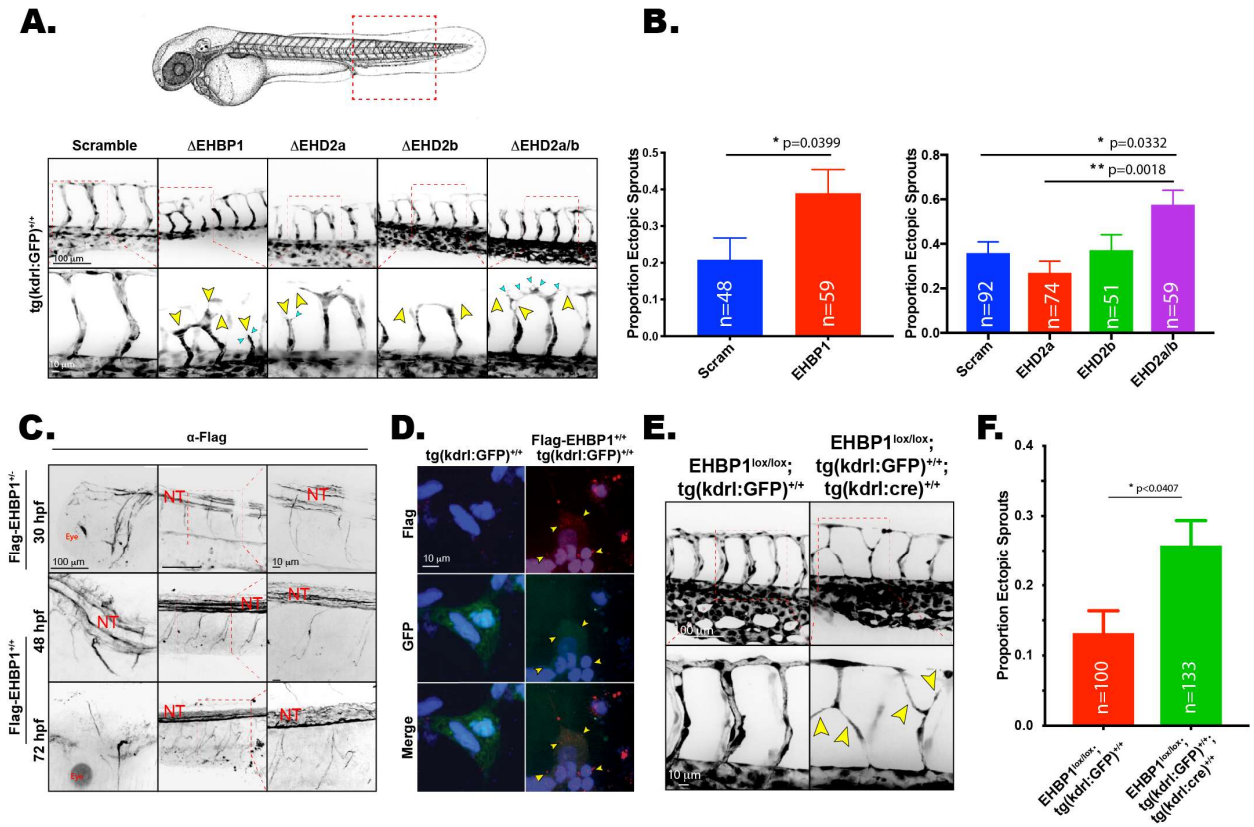

Figure 1. EHBP1 and EHD2 promote ectopic sprouting in zebrafish blood vessels. (A) Red dashed box denotes area of imaging. 4-guide knockout (KO) fish were imaged on tg(kdrl:GFP)$^{+/+}$ background at 48 hpf. Yellow arrows denote abnormal vascular growth. Teal arrows point to spiny projections. (B) Quantification of the proportion of 4-guide KO fish with ectopic ISVs. Ectopic was defined as a vessel projection emerging from the ISV distinct from the central stalk. (C) Staining against FLAG epitope in various stages of development highlighting expression in the neural tube (NT) in indicated genotypes. (D) Ex vivo validation of expression of FLAG-EHBP1 in endothelial cells. Yellow arrows denote areas of FLAG positivity. (E) Representative images of ISVs in indicated genotypes. Yellow arrows denote abnormal vascular growth. (F) Quantification of proportion of fish with ectopic ISVs. Error bars represent SEM. n= number of fish quantified.

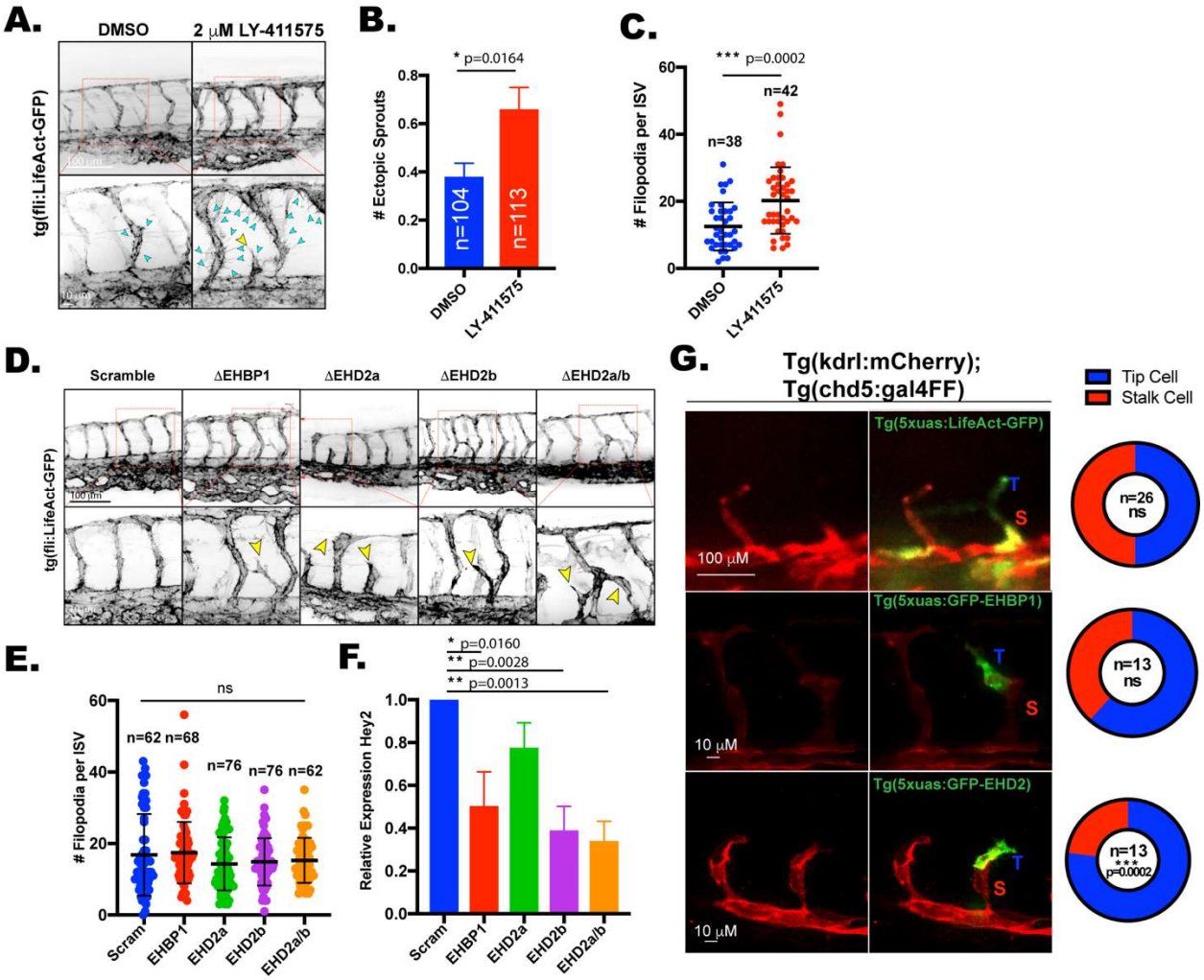

Figure 2. EHBP1 and EHD2 knockouts phenocopy Notch loss of function. (A) ISVs of fish treated with either DMSO or 2 μM LY-411575 on tg(fli:LifeAct)$^{+/+}$ background. Yellow arrows point to ectopic sprouts. Teal arrows point to filopodial projections. (B) Number of ectopic ISVs per fish between indicated groups. (C) Number of ISV filopodial extensions between indicated groups. (D) Representative images of 4-guide KO of EHBP1 and EHD2 on tg(fli:LifeAct-GFP)$^{+/+}$ background. Yellow arrows point to ectopic sprouts. (E) Number of ISV filopodial extensions among indicated groups. (F) Relative expression of Hey2 transcript in 48hpf 4-guide KO fish compared to GAPDH control across indicated groups. (G) Representative images of GFP-EHD2, GFP-EHBP1, and LifeAct-GFP overexpression constructs in growing ISVs at 24 hpf. Quantification of the proportion of expressing endothelial cells in either the tip (T, blue) or stalk (S, red) cell position in the growing vascular sprouts shown to the right. n= number of fish, ns= non-significant. Error bars represent SEM in (B) and (F) and SD in (C) and (E).

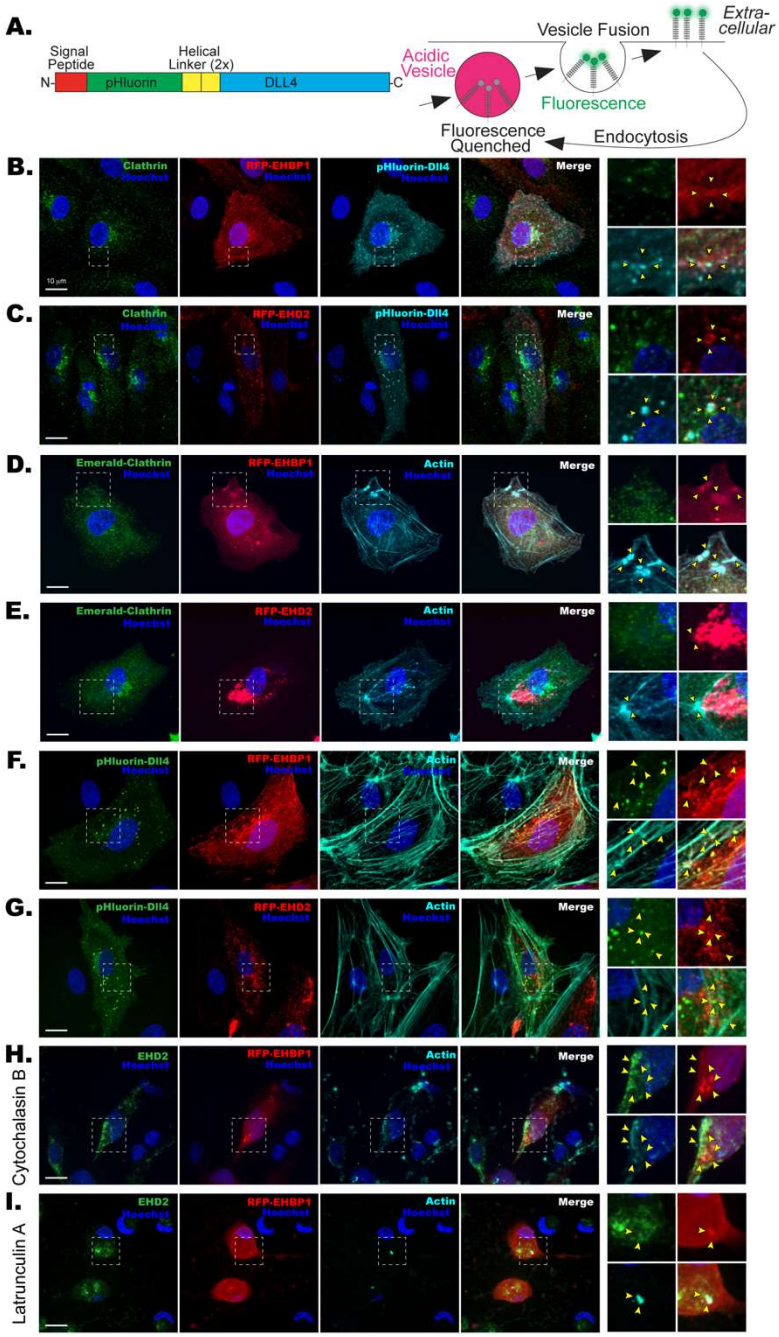

Figure 3. Endothelial Dll4 does not localize with EHBP1 and EHD2 on clathrin endocytic pits. (A) Schematic of pH-dependent function of GFP variant pHluorin tag. PHluorin fluoresces on the membrane at neutral pH, but is quenched when internalized into acidic endosomes. (B) EHBP1 localizes around sites of pHluorin-Dll4 independent of clathrin. (C) EHD2 localizes around sites of pHluorin-Dll4 independent of clathrin. (D,E) EHBP1 and EHD2 localized to sites of F-actin bundling independent of clathrin. (F,G) EHBP1 and EHD2 cluster around Dll4 puncta at sites of F-actin bundling. (H,I) Actin inhibitors Cytochalasin B and Latrunculin A disrupt EHBP1 and EHD2 localization. Boxed are magnified section on right. Yellow arrows show areas of colocalization.

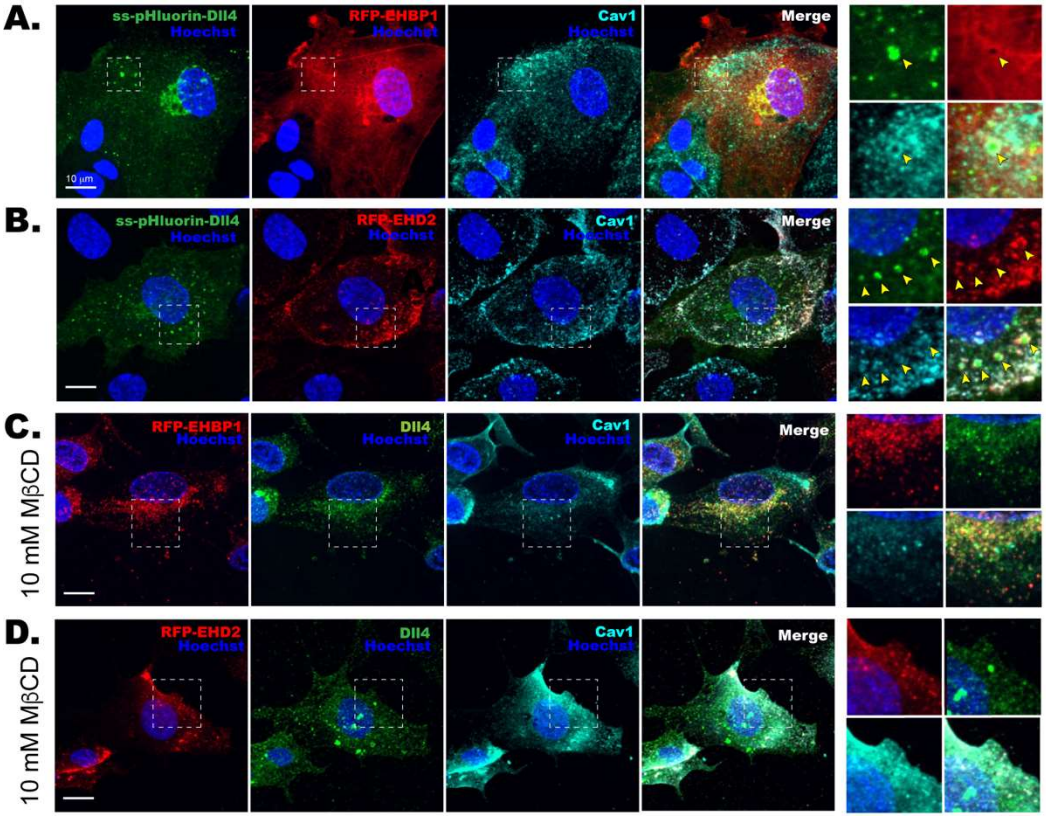

Figure 4. Endothelial Dll4 localizes with EHBP1 and EHD2 on caveolin endocytic pits. (A,B) EHBP1 and EHD2 localize to surface pHluorin-Dll4 and colocalize with caveolin-1. (C) EHBP1 and (D) EHD2 fail to localize to Dll4 when treated with MβCD (cholesterol inhibitor). Boxed are magnified section on right. Yellow arrows show areas of colocalization.

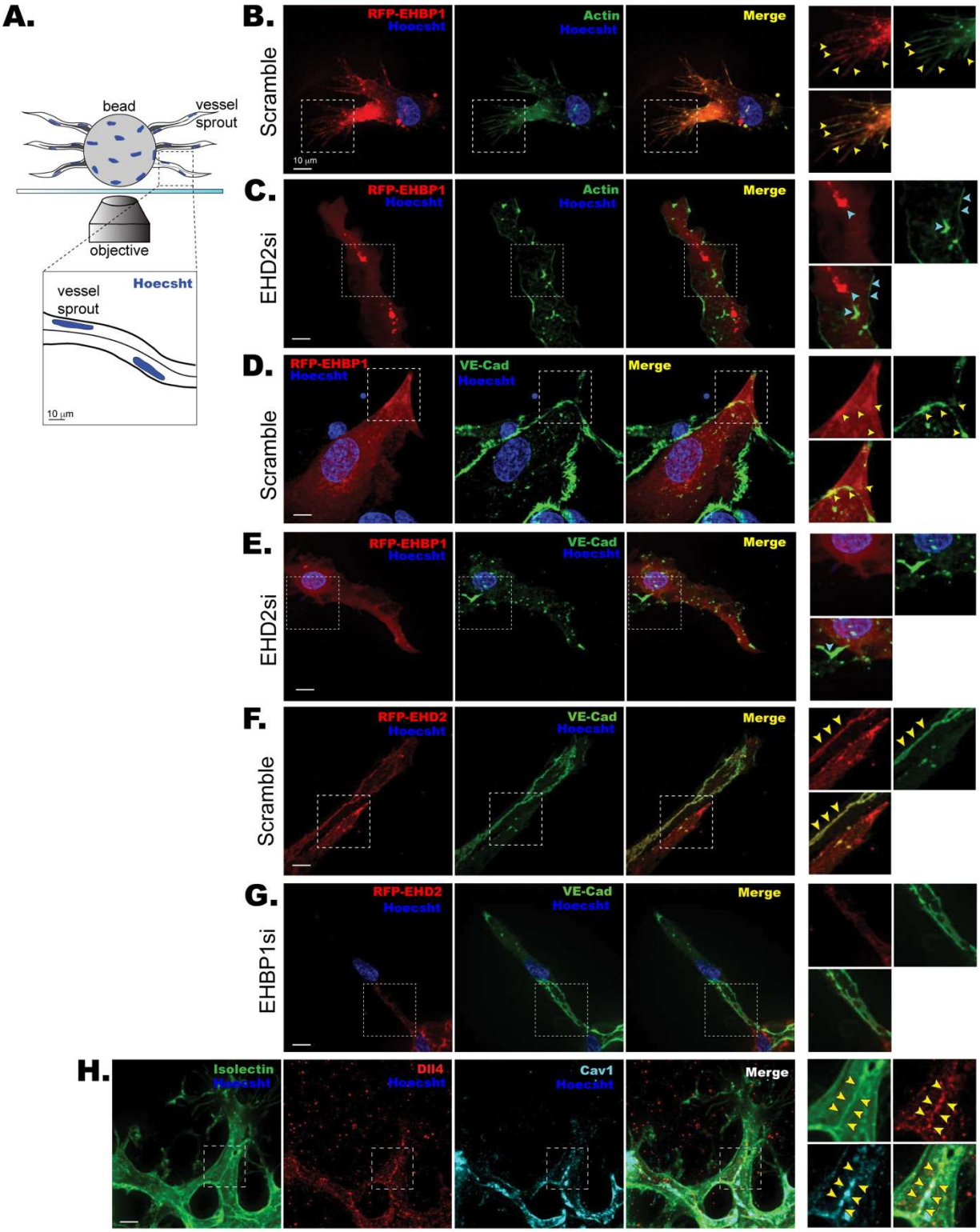

Figure 5. EHBP1, EHD2, and caveolin localize to adherens junctions in 3D sprouts. (A) Schematic of 3-dimensional sprout growth in fibrin bead assay (FBA). (B,C) Representative EC sprout stained for actin expressing tagRFP-EHBP1, treated with indicated siRNA. (D,E)

Representative EC sprout stained for VE-cadherin (VE-cad) expressing tagRFP-EHBP1, treated with indicated siRNA. (F,G) Representative EC sprout stained for VE-cadherin (VE-cad) expressing tagRFP-EHD2, treated with indicated siRNA. (H) Dll4 and caveolin-1 colocalize at adherens junction in P6 mouse retinal blood vessels. Boxed are magnified section on right. Yellow arrows show areas of colocalization. Teal arrows show areas of mislocalization.

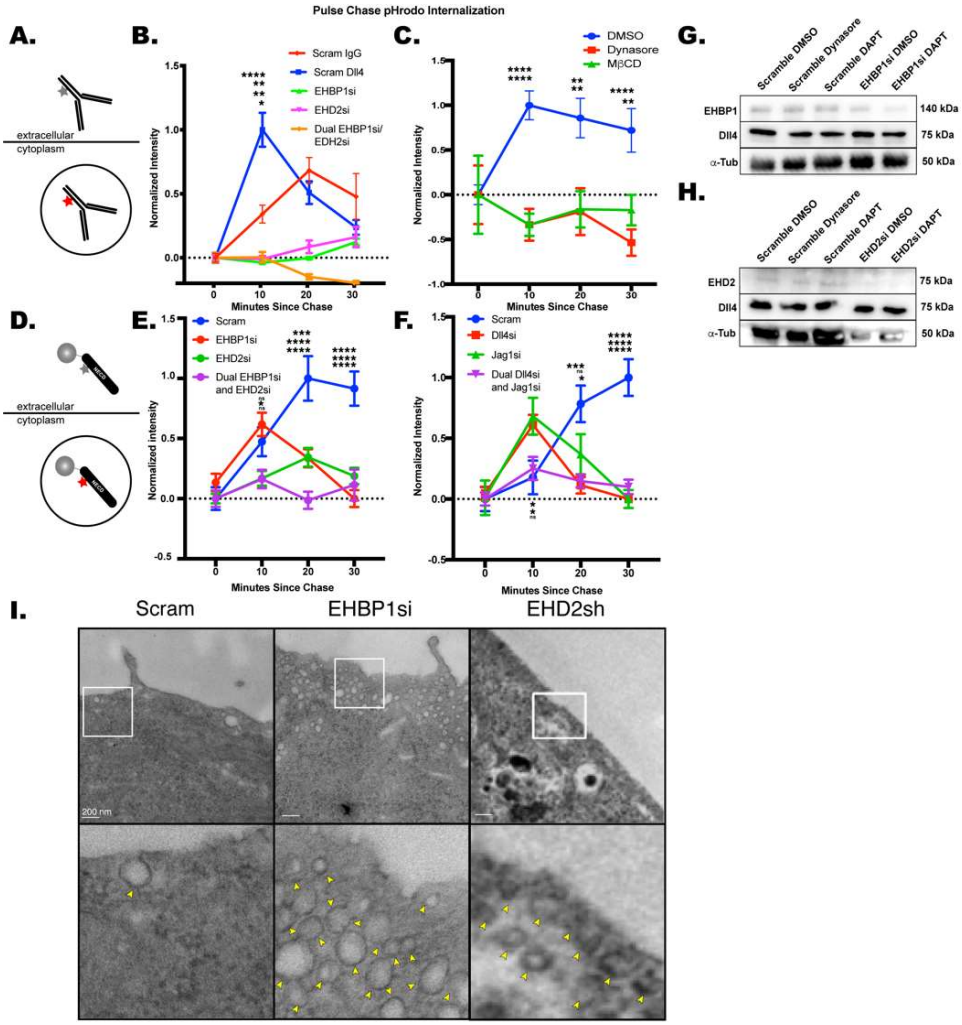

Figure 6. Loss of EHBP1 and EHD2 blunts Dll4 endocytosis. (A) Schematic of pHrodo labeled Dll4 antibody. PHrodo gains fluorescent intensity with increasing endosomal pH, thus used as a metric of endocytosis. (B,C) Relative internalization of pHrodo-Dll4 pulse-chase over time between indicated siRNA groups. IgG was used a non-specific internalization control. Dynasore is pan-endocytosis inhibitor. MβCD is a cholesterol specific inhibitor that disrupts caveolin. (D) Schematic recombinant Notch intracellular domain (NECD) functionalized to microbead and labeled with pHrodo. (E,F) Relative internalization of NECD pulse-chase over time between indicated siRNA groups. (G,H) Western blot of Dll4 levels across indicated treatment groups. (I) TEM analysis of caveolar structure in ECs in across indicated siRNA treatments. White inset boxes show area of magnification. Yellow arrowheads indicate endocytic vacuoles. Significance between scramble group and other groups listed in order of figure legend. *=p<0.05, **=p<0.01, ***=p<0.001, ****=p<0.0001. ns=non-significant.

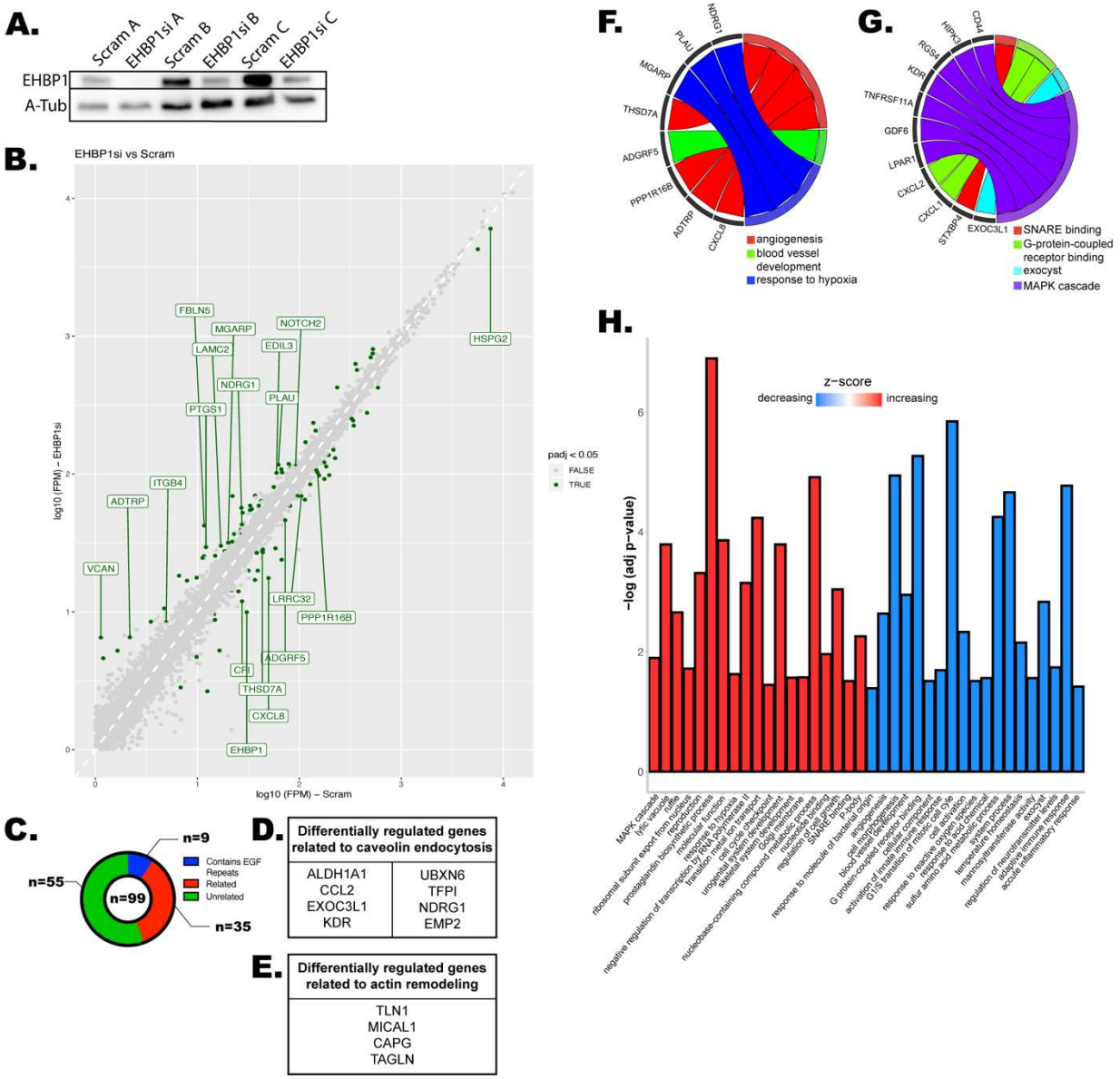

Figure 7. RNA-seq Analysis of EHBP1si treated cells. (A) Confirmation of knockdown efficiency of EHBP1 siRNA replicates. (B) Volcano plot distribution of all differentially regulated genes in EHBP1si condition compared to control. Dots above the line represent upregulation; dots below the line represent downregulation. Dark green dots represent significantly differentially regulated genes. Highlighted points are relevant to angiogenic signaling. (C) Number of significantly different transcripts that contain EGF repeat motifs, are (D) directly related to caveolin-mediated endocytosis or (E) directly related to actin remodeling. (F) Significantly differentially regulated genes related to angiogenesis. (G) Significantly differentially regulated to endo- or exocytosis. (H) All gene ontology groupings of significantly differentially regulated genes. Bars shown in red were upregulated as a group. Bars shown in blue were downregulated as a group.

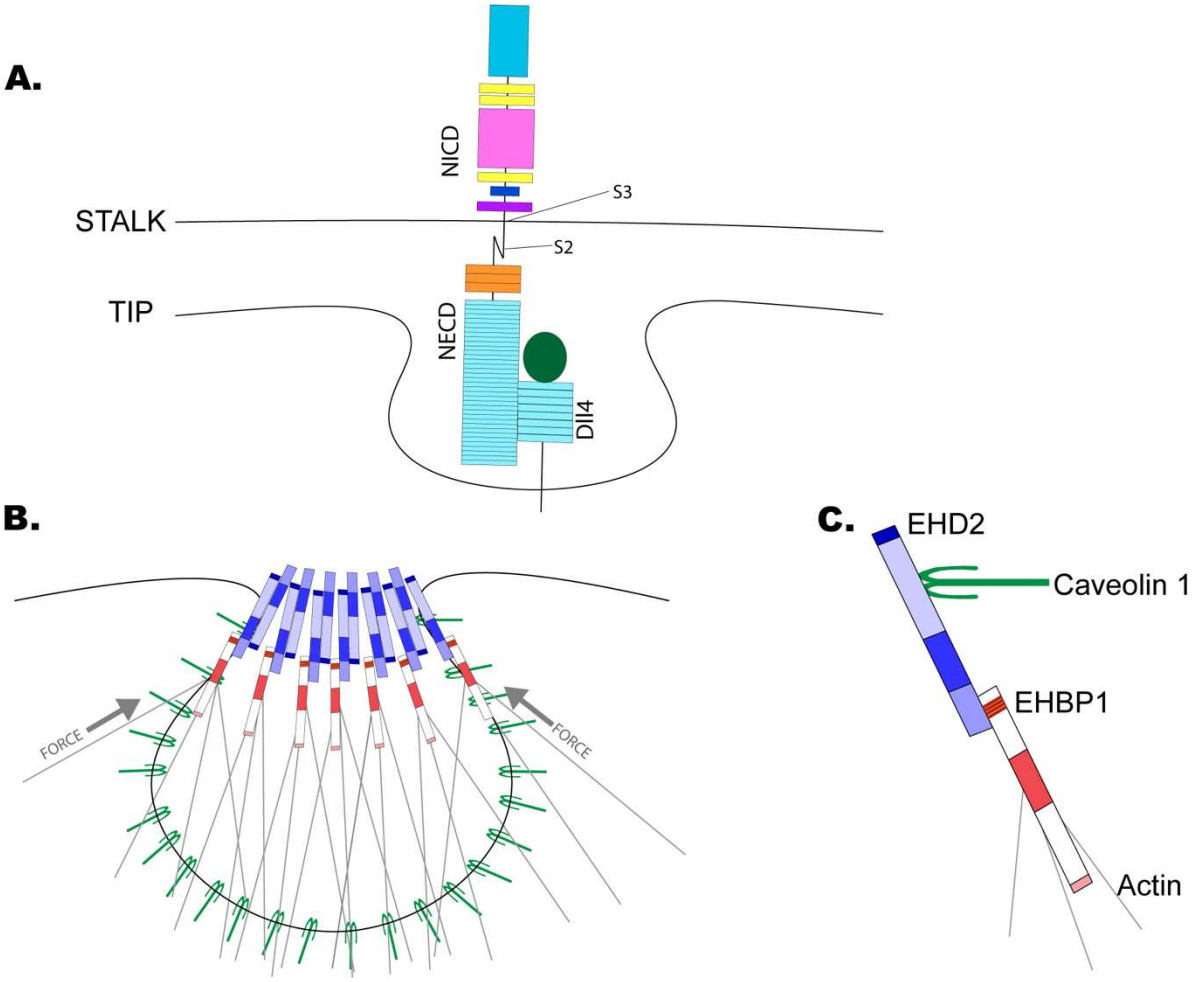

Figure 8. **Model of EHBP1 and EHD2 mediated Dll4 internalization.** (A) Dll4 binds NECD in the budding caveolin pit. (B,C) EHD2 binds caveolin and oligomerizes around the neck of the endocytic pit. EHBP1 binds to EHD2 and tethers to the actin cytoskeleton through the CH domain. This may generate the force necessary to expose the S2 cleavage site of Notch.

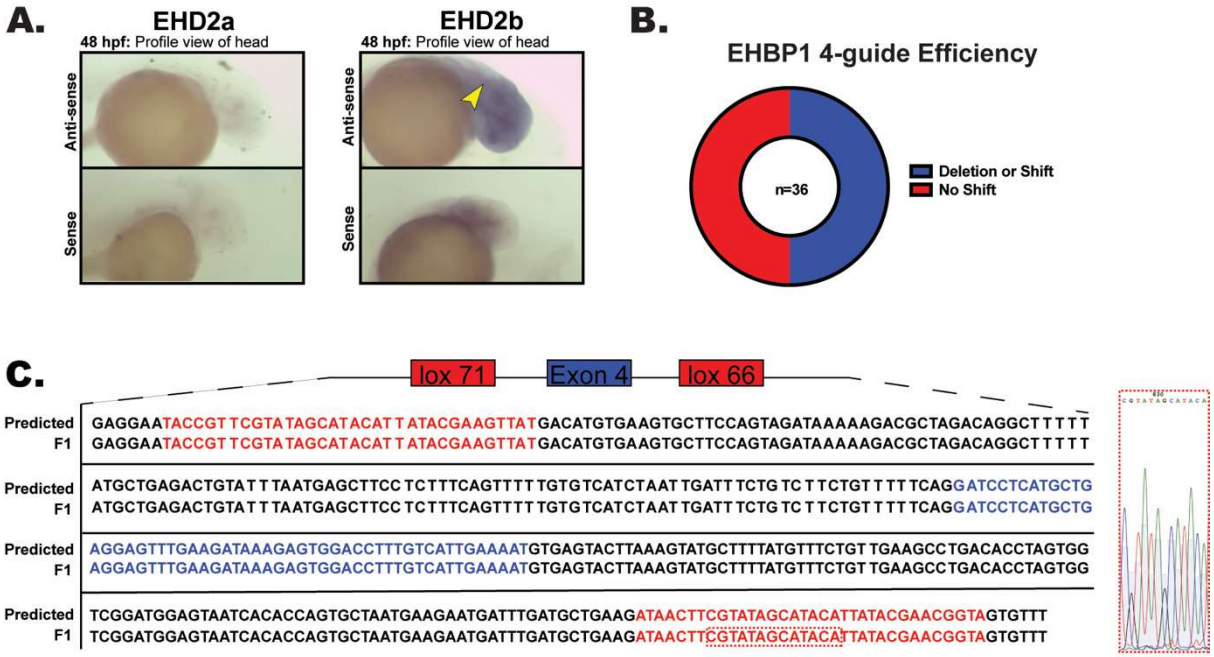

Figure S1. Confirmation of in vivo genetic tools. (A) In situ hybridization against either EHD2a or EHD2b. Yellow arrow points to expression along neural tube. (B) PCR of sites around 3 of the 4 guides used in the EHBP1 knockout demonstrate that half of 36 sampled fish had deletions or shifts of approximately greater than or equal to 100 bp. Smaller deletions undetected in this assay. (C) Confirmation of in frame lox site incorporation into F1 generation EHBP1 floxed fish. Predicted sequence shown in first row, sequenced F1 fish shown in second row. Sanger sequencing peaks of small region in c-terminal lox site highlighted to the right.

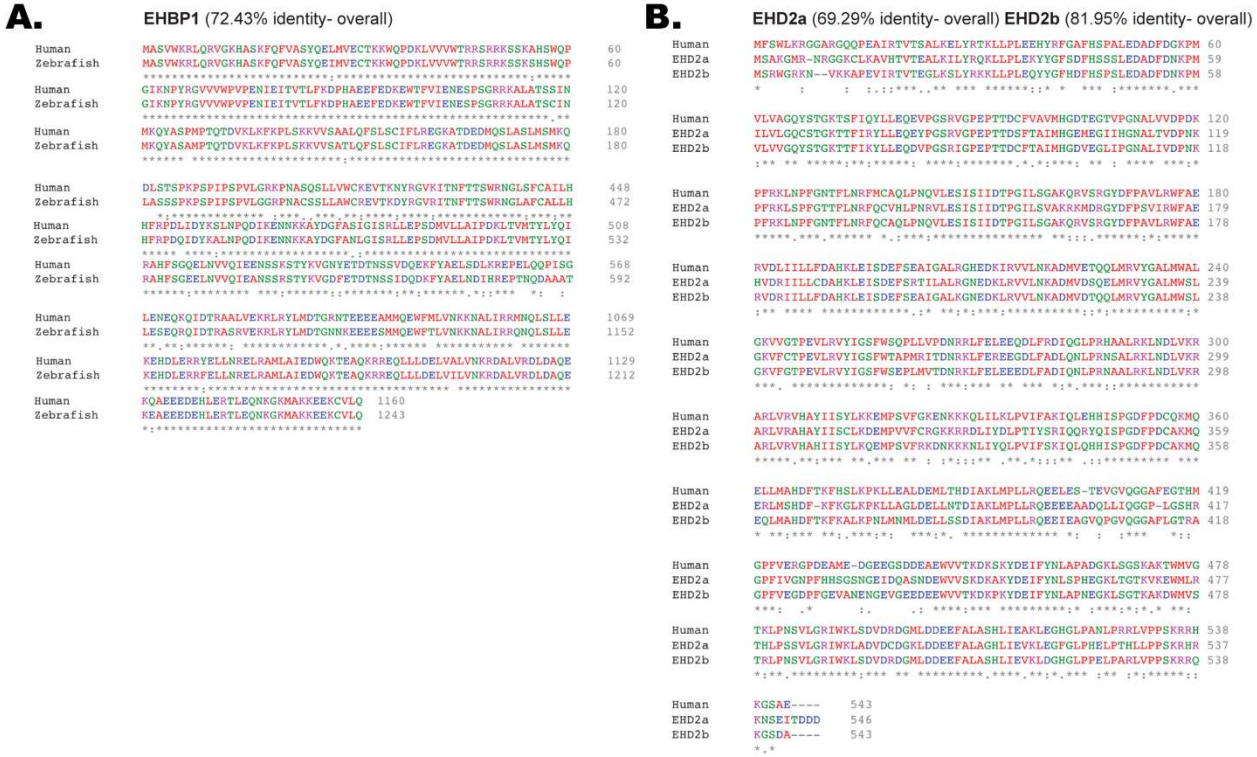

Figure S2. Comparison of EHBP1 and EHD2 amino acid identity between Human and Zebrafish. (A) Amino acid alignment of Human and Zebrafish EHBP1. (B) Amino acid alignment of Human EHD2 and zebrafish EHD2a or b.

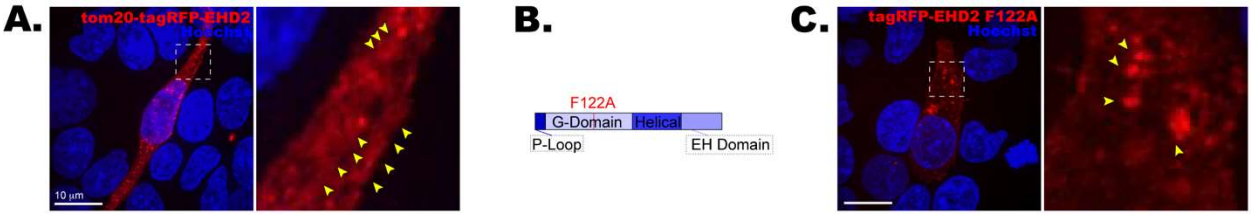

Figure S3. EHD2 mutants fail to form organized rosettes. (A) N-terminal tom20 tag localizes EHD2 to fragmented mitochondria in HEK 293 cells (yellow arrows). (B) Schematic of F122A mutation to EHD2 in the G-domain responsible for oligomerization. (C) EHD2 F122A mutant is primarily diffuse in the cytoplasm of HEK 293 cells, with some punctate clustering (yellow arrows) failing to form rosette structures.

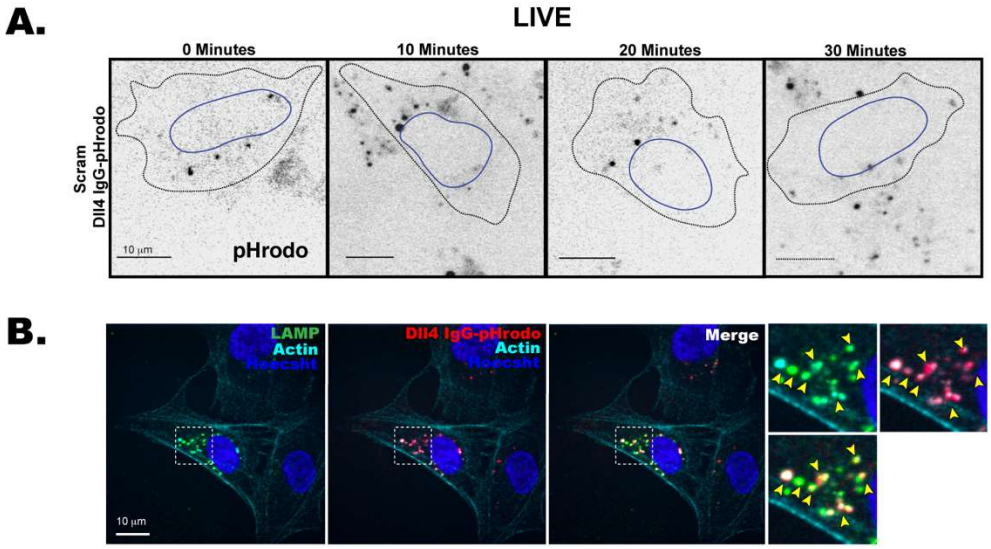

Figure S4. Dll4 IgG-pHrodo trafficks to lysosome. (A) Representative images of individual ECs internalizing pHrodo-Dll4 over time. pHrodo shown is black puncta. (B) Phrodo-treated ECs stained for lysosomal marker LAMP and actin. Yellow arrows show colocalization.

	baseMean	log2FoldChange	lfcSE	stat	pvalue	padj	symbol
ENSG00000089723	22.1014999	-4.63E+00	1.13612207	-4.0720217	4.66E-05	NA	OTUB2
ENSG00000183840	27.3967476	-3.15E+00	0.85943631	-3.6656858	0.00024668	3.52E-02	GPR39
ENSG00000157045	171.041544	-1.99E+00	0.36389978	-5.4718281	4.45E-08	2.17E-05	NTAN1
ENSG00000115504	473.845438	-1.73E+00	0.22589519	-7.6578629	1.89E-14	4.80E-11	EHBP1
ENSG00000081041	242.551212	-1.59E+00	0.27410654	-5.7860868	7.20E-09	5.38E-06	CXCL2
ENSG00000169429	764.532758	-1.55E+00	0.1774785	-8.7351553	2.43E-18	1.03E-14	CXCL8
ENSG00000163131	182.37218	-1.54E+00	0.34081567	-4.5207608	6.16E-06	1.78E-03	CTSS
ENSG00000163739	1040.71362	-1.46E+00	0.22843278	-6.385674	1.71E-10	1.97E-07	CXCL1
ENSG00000010319	632.589134	-1.22E+00	0.2171759	-5.6369928	1.73E-08	1.14E-05	SEMA3G
ENSG00000205403	451.260567	-1.18E+00	0.21285323	-5.5305096	3.19E-08	1.69E-05	CFI
ENSG00000120337	1000.91183	-1.03E+00	0.15505798	-6.6528189	2.88E-11	4.56E-08	TNFSF18
ENSG00000165092	3357.86352	-1.02E+00	0.12647914	-8.0326286	9.54E-16	3.03E-12	ALDH1A1
ENSG00000158270	672.056722	-9.71E-01	0.17238019	-5.6302976	1.80E-08	1.14E-05	COLEC12
ENSG00000108691	3071.1138	-9.70E-01	0.16099826	-6.0263488	1.68E-09	1.42E-06	CCL2

ENSG00000141655	271.839886	-9.27E-01	0.25456054	-3.6428714	0.00026961	3.68E-02	TNFRSF11A
ENSG00000165801	275.612365	-8.97E-01	0.24951248	-3.5952761	0.00032405	4.24E-02	ARHGEF40
ENSG00000111339	449.594481	-8.34E-01	0.20054603	-4.1573446	3.22E-05	7.29E-03	ART4
ENSG00000179044	597.448679	-8.32E-01	0.18207129	-4.5714542	4.84E-06	1.46E-03	EXOC3L1
ENSG00000185339	2045.81482	-8.26E-01	0.13540518	-6.0974007	1.08E-09	9.77E-07	TCN2
ENSG00000205502	819.148073	-8.20E-01	0.22562937	-3.632243	0.00028097	3.79E-02	C2CD4B
ENSG00000151012	4060.63317	-7.76E-01	0.14666717	-5.2879169	1.24E-07	5.61E-05	SLC7A11
ENSG00000137507	1984.79427	-7.73E-01	0.13753493	-5.620421	1.90E-08	1.15E-05	LRRC32
ENSG00000128918	420.821593	-7.60E-01	0.20193262	-3.7650566	0.00016651	2.74E-02	ALDH1A2
ENSG00000005108	803.863033	-7.42E-01	0.1664832	-4.4566431	8.33E-06	2.30E-03	THSD7A
ENSG00000154222	924.924761	-7.37E-01	0.20311171	-3.6263785	0.00028742	3.84E-02	CC2D1B
ENSG00000159640	2833.08572	-7.27E-01	0.13001192	-5.5949959	2.21E-08	1.22E-05	ACE
ENSG00000182621	743.292897	-7.11E-01	0.19503798	-3.6437596	0.00026868	3.68E-02	PLCB1
ENSG00000128052	8404.32115	-7.00E-01	0.1136694	-6.1620562	7.18E-10	7.01E-07	KDR
ENSG00000069122	1349.65009	-6.75E-01	0.14560161	-4.6333794	3.60E-06	1.11E-03	ADGRF5

ENSG00000112096	3514.23599	-6.68E-01	0.17974848	-3.7164804	0.00020202	3.07E-02	SOD2
ENSG00000170323	1881.10706	-6.45E-01	0.1546985	-4.1698611	3.05E-05	7.03E-03	FABP4
ENSG00000189221	824.77486	-6.42E-01	0.16453121	-3.9042183	9.45E-05	1.82E-02	MAOA
ENSG00000185070	3810.78858	-6.05E-01	0.14115872	-4.2865627	1.81E-05	4.70E-03	FLRT2
ENSG00000101445	2880.30759	-5.68E-01	0.12449194	-4.5630315	5.04E-06	1.49E-03	PPP1R16B
ENSG00000100906	1598.15353	-5.52E-01	0.14284274	-3.8665744	0.00011038	2.03E-02	NFKBIA
ENSG00000120885	4198.03674	-5.42E-01	0.12752303	-4.2472826	2.16E-05	5.42E-03	CLU
ENSG00000125266	2397.97689	-5.16E-01	0.1360608	-3.7903846	0.00015041	2.62E-02	EFNB2
ENSG00000173852	3386.38156	-4.96E-01	0.13157754	-3.7689363	0.00016395	2.74E-02	DPY19L1
ENSG00000167671	2455.64308	-4.89E-01	0.13311375	-3.6743535	0.00023845	3.48E-02	UBXN6
ENSG00000140105	6448.63426	-4.87E-01	0.12091255	-4.0288764	5.60E-05	1.17E-02	WARS1
ENSG00000137509	6604.07757	-4.87E-01	0.11862697	-4.1015272	4.10E-05	8.98E-03	PRCP
ENSG00000113555	1551.34199	-4.85E-01	0.13618446	-3.5606847	0.00036989	4.74E-02	PCDH12
ENSG00000130309	11541.5449	-4.65E-01	0.10815847	-4.3006895	1.70E-05	4.60E-03	COLGALT1
ENSG00000091490	2844.23249	-4.64E-01	0.12452639	-3.7229279	0.00019693	3.07E-02	SEL1L3

ENSG00000110799	111048.992	-4.42E-01	0.1029534	-4.2928171	1.76E-05	4.66E-03	VWF
ENSG00000003436	6639.33473	-4.16E-01	0.11516043	-3.6103013	0.00030584	4.04E-02	TFPI
ENSG00000142798	150415.616	-3.89E-01	0.10621257	-3.6659041	0.00024647	3.52E-02	HSPG2
ENSG00000124762	7670.1264	4.15E-01	0.11337507	3.66028578	0.00025193	3.55E-02	CDKN1A
ENSG00000182492	13726.0988	4.53E-01	0.11192617	4.0483092	5.16E-05	1.09E-02	BGN
ENSG00000134250	2345.1412	5.12E-01	0.13528724	3.78209148	0.00015552	2.67E-02	NOTCH2
ENSG00000166073	1558.61309	5.18E-01	0.14084313	3.6758658	0.00023704	3.48E-02	GPR176
ENSG00000149948	4044.85411	5.52E-01	0.11810873	4.67713976	2.91E-06	9.46E-04	HMGA2
ENSG00000152377	14633.1236	5.67E-01	0.12096004	4.69093988	2.72E-06	9.08E-04	SPOCK1
ENSG00000106624	3258.23347	5.68E-01	0.11945835	4.75291138	2.01E-06	7.07E-04	AEBP1
ENSG00000026508	2248.14992	5.73E-01	0.14296751	4.00554371	6.19E-05	1.27E-02	CD44
ENSG00000173597	2273.77964	5.73E-01	0.15704098	3.64937447	0.00026288	3.66E-02	SULT1B1
ENSG00000163453	10657.3348	5.89E-01	0.10847826	5.4309934	5.60E-08	2.63E-05	IGFBP7
ENSG00000137076	15256.9275	6.31E-01	0.11173934	5.64404327	1.66E-08	1.14E-05	TLN1
ENSG00000135596	763.813419	6.64E-01	0.16387353	4.05007799	5.12E-05	1.09E-02	MICAL1

ENSG00000136205	1965.21818	6.70E-01	0.16006608	4.18425307	2.86E-05	6.80E-03	TNS3
ENSG00000102802	1022.89021	6.72E-01	0.16063164	4.18144251	2.90E-05	6.80E-03	MEDAG
ENSG00000137463	591.931053	6.79E-01	0.18210269	3.72801379	0.000193	3.07E-02	MGARP
ENSG00000164237	744.6505	6.87E-01	0.18465221	3.71976233	0.00019941	3.07E-02	CMBL
ENSG00000058729	661.623394	6.92E-01	0.1780192	3.88508294	0.0001023	1.91E-02	RIOK2
ENSG00000104419	813.844009	7.20E-01	0.18821135	3.8233801	0.00013164	2.35E-02	NDRG1
ENSG00000213853	534.861358	7.31E-01	0.20376671	3.58613329	0.00033562	4.34E-02	EMP2
ENSG00000176438	626.176204	7.41E-01	0.18613628	3.98051737	6.88E-05	1.36E-02	SYNE3
ENSG00000042493	1232.92484	7.51E-01	0.16794293	4.47117265	7.78E-06	2.19E-03	CAPG
ENSG00000164176	1846.00677	7.51E-01	0.14914398	5.03662689	4.74E-07	1.82E-04	EDIL3
ENSG00000058085	537.388406	7.53E-01	0.20303128	3.70996898	0.00020729	3.09E-02	LAMC2
ENSG00000110422	1148.78248	7.53E-01	0.20281268	3.71483592	0.00020334	3.07E-02	HIPK3
ENSG00000128567	11224.646	7.54E-01	0.14876757	5.06628173	4.06E-07	1.61E-04	PODXL
ENSG00000170017	4245.17267	7.75E-01	0.13135229	5.9018274	3.59E-09	2.85E-06	ALCAM
ENSG00000128606	463.967334	7.87E-01	0.20841935	3.77529963	0.00015982	2.70E-02	LRRC17

ENSG00000257103	1011.24753	8.03E-01	0.18945659	4.23799976	2.26E-05	5.50E-03	LSM14A
ENSG00000100979	1043.9293	8.26E-01	0.16175581	5.10843024	3.25E-07	1.37E-04	PLTP
ENSG00000167244	672.855837	8.31E-01	0.17640768	4.70840377	2.50E-06	8.56E-04	IGF2
ENSG00000122861	2039.71415	8.49E-01	0.13724269	6.18881744	6.06E-10	6.41E-07	PLAU
ENSG00000070404	907.394343	8.50E-01	0.17565711	4.8402049	1.30E-06	4.84E-04	FSTL3
ENSG00000136928	318.037015	8.82E-01	0.230182	3.8320666	0.00012707	2.30E-02	GABBR2
ENSG00000135480	7541.39705	8.86E-01	0.1274009	6.95684172	3.48E-12	6.31E-09	KRT7
ENSG00000117152	1998.0236	8.94E-01	0.13707658	6.52432894	6.83E-11	9.63E-08	RGS4
ENSG00000134668	1208.86968	9.06E-01	0.16184649	5.59948036	2.15E-08	1.22E-05	SPOCD1
ENSG00000055163	414.539763	9.85E-01	0.20676131	4.76392303	1.90E-06	6.88E-04	CYFIP2
ENSG00000142173	282.89198	1.01E+00	0.25334933	3.97164385	7.14E-05	1.39E-02	COL6A2
ENSG00000115107	406.782247	1.09E+00	0.20634744	5.27535593	1.32E-07	5.80E-05	STEAP3
ENSG00000156466	174.801706	1.13E+00	0.29087678	3.89531747	9.81E-05	1.86E-02	GDF6
ENSG00000166263	300.420972	1.15E+00	0.30746465	3.72566798	0.0001948	3.07E-02	STXBP4
ENSG00000172260	971.078177	1.18E+00	0.15493531	7.59557985	3.06E-14	6.48E-11	NEGR1

ENSG00000169282	136.94956	1.24E+00	0.3281543	3.78999393	0.00015065	2.62E-02	KCNAB1
ENSG00000095303	480.096711	1.27E+00	0.19689882	6.46808397	9.93E-11	1.26E-07	PTGS1
ENSG00000132470	157.422906	1.27E+00	0.31945966	3.98815633	6.66E-05	1.34E-02	ITGB4
ENSG00000162490	283.662047	1.41E+00	0.25686768	5.47408984	4.40E-08	2.17E-05	DRAXIN
ENSG00000149591	1053.8429	1.72E+00	0.18537703	9.25936363	2.06E-20	1.30E-16	TAGLN
ENSG00000198121	81.8514719	1.77E+00	0.41757138	4.24568193	2.18E-05	5.42E-03	LPAR1
ENSG00000111863	103.548945	1.78E+00	0.38418903	4.64077259	3.47E-06	1.10E-03	ADTRP
ENSG00000140092	614.921263	1.89E+00	0.18470883	10.2580904	1.09E-24	1.38E-20	FBLN5
ENSG00000198768	67.17495	2.00E+00	0.48231197	4.14023541	3.47E-05	7.72E-03	APCDD1L
ENSG00000074047	48.9564553	2.55E+00	0.68282283	3.72863732	0.00019252	3.07E-02	GLI2
ENSG00000038427	93.1004752	2.60E+00	0.51313274	5.06633197	4.06E-07	1.61E-04	VCAN

Table S1. Significantly differentially regulated genes between EHBP1si and Scramble groups.

Contain EGF repeats	Related to EGF signaling
LRRC32	GPR39
HSPG2	EHBP1
Notch2	CXCL2
EDIL3	CXCL8
LAMC2	CTSS
PTGS1	CXCL1
ITGB4	SEMA3G
FBLN5	CCL2
VCAN	THSD7A
	CC2D1B
	ACE
	KDR
	ADGRF5
	FABP4
	MAOA
	FLRT2
	PPP1R16B
	NFKBIA
	EFNB2
	DPY19L1
	TFPI
	BGN
	GPR176
	HMGA2
	CD44
	IGFBP7
	MICAL1
	TNS3
	NDRG1
	EMP2
	SPOCD
	NEGR1
	DRAXIN
	LPAR1
	GLI2

Table S2. List of differentially related genes containing EGF repeats or related to EGF signaling.